Title: Reducing the global human footprint on lake water quality near river inlets

Authors: Benjamin M. Kraemer[1], Sami Domisch[2], Jaime R. Garcia Marquez[2], Catalina Munteanu[3,4], Shahrokh Shahbazi[5], Sapna Sharma[6], Kerstin Stahl[1], Michael W. Thayne[7], Thomas Tomiczek[2], Janis M. Wolf[8]

Affiliations:

[1] University of Freiburg, Environmental Hydrological Systems, Freiburg, Germany

[2] Leibniz Institute of Freshwater Ecology and Inland Fisheries (IGB), Department of Community and Ecosystem Ecology, Berlin, Germany

[3] University of Freiburg, Wildlife Ecology and Management, Freiburg, Germany

[4] Swiss Federal Institute for Forest, Snow and Landscape Research WSL

[5] TH Köln – University of Applied Sciences, Institute for Technology and Resources Management in the Tropics and Subtropics (ITT), Cologne, Germany

[6] York University, Department of Biology, Toronto, Canada

[7] GFZ German Research Centre for Geosciences, Remote Sensing Section, Potsdam, Germany

[8] University of Greifswald, Zoological Institute and Museum, Greifswald, Germany

[[[This manuscript is a non-peer reviewed preprint submitted to EarthArXiv]]]

[[[It has not yet been submitted to a journal for peer review]]]

Abstract: Human activities have degraded lake water quality globally, leading to toxic algae proliferation and anoxia. The spatial variability of these impacts within lakes and the potential for targeted nutrient pollution reduction to improve water quality remain however underexplored at the global scale. Using 742 million chlorophyll-a (chl-a) estimates from six satellite sensors (daily, 1–4 km resolution), we mapped surface chl-a across 321 large lakes, averaged over the time interval from 1997 to 2020. We bias-corrected these data through lake-specific algorithm tuning based on morphometric characteristics and in-situ water samples. Our analysis revealed distinct spatial patterns in chl-a concentrations within lakes, with the highest concentrations often occurring near river inflows, driven primarily by nutrient pollution from croplands. Importantly, we found that reductions in chl-a concentrations can be achieved across latitudes by minimizing agricultural nutrient inputs, with lower-latitude lakes across Africa, South America, and Asia, exhibiting the largest potential for reductions in chl-a concentrations and improved water quality. However, reductions in nutrient pollution may have limited influence on chl-a concentrations in open waters, suggesting that nearshore areas, which often support higher biodiversity, may benefit most from targeted interventions. These findings underscore the importance of spatially explicit management strategies to address the varying impacts of nutrient pollution across and within lakes.

Main Text: Intensifying nutrient runoff, climatic warming, and pollution from human activities are driving widespread and cascading declines in lake water quality globally [1,2]. These impacts are largely fueled by the introduction of excess nutrients, particularly nitrogen and phosphorus, which promote eutrophication [2]. Agricultural activities are widely recognized as the primary driver of global lake water quality degradation [3,4]. However, sewage and urban runoff can contribute stronger to nutrient sources driving eutrophication in regions with lower agricultural intensity and poor wastewater management [5]. Thus, contemporary global differences in both agricultural intensity and other nutrient pollution sources may shape regional and global variation in the drivers of lake water quality degradation. Understanding where and how these pressures manifest within individual lakes is essential to accurately assess their ecological consequences.

Eutrophication can be a lakewide phenomenon, but in many cases, its impacts are more concentrated near shorelines, particularly around river inflows [6]. Despite this spatial heterogeneity, long-term lake monitoring typically focuses only on central or deepest points in lakes [7], a practice that often stems from the need to characterize the lake's entire water column in terms of its various ecological gradients. At times, surface measurements from these central

points suggest slower or less pronounced declines in water quality, giving the impression that human impacts are weaker than they actually are near shore[8,9] however, these sampling points are generally far from inflowing rivers where nutrient pollution impacts at the surface are likely most severe. Even in small lakes, lateral heterogeneity in lake properties can be surprisingly large [10,11]. Thus, limnological sampling norms focused on central or deepest points may limit our capacity to detect the real influence of terrestrial human activities on water quality. The use of integrated, high-resolution spatial and temporal monitoring approaches, including remote sensing, would provide a more comprehensive view of how nutrient pollution impacts lakes. This would allow for more targeted management strategies, such as buffer zones, riparian vegetation restoration, and improved nutrient management practices in upstream agricultural areas.

To effectively target nutrient pollution reduction efforts, two flawed assumptions in monitoring and management must be addressed: (1) that agriculture is the primary driver of lake water quality degradation globally, and (2) that offshore water quality adequately represents conditions across the entire lake. These assumptions can obscure a full understanding of the drivers and spatial patterns of human impacts on global lake water quality. In this study, we explicitly address both biases by examining the drivers of within lake variation in lake water quality, quantifying how their relative influence varies across the globe, and assessing how water quality degradation diminishes with distance from the mouths of major rivers. By addressing these assumptions, we provide a more nuanced perspective on the spatial patterns of human impacts within and across lakes, enabling more targeted and effective nutrient pollution management strategies. We used 742 million chl-a estimates from six satellite sensors (daily, 1 to 4 km resolution) to map average chl-a in 321 large lakes distributed globally (ranging in surface area from 100 to 377002 km^2) from the year 1997 to 2020 (Fig. 1). These remote sensing data were bias-corrected using in situ water sample extractions, tuning the chl-a algorithm for each lake based on its characteristics such as depth, surface area, and residence time [6]. We used a machine learning algorithm (boosted regression trees; BRT) to predict spatial variation in temporally averaged chl-a estimates within lakes using predictors including watershed cropland extent, pastureland extent, urban extent, population count, human development index, air temperature, evapotranspiration, elevation, silt extent, karst extent, groundwater table depth, wetland extent, and two within-lake location variables (distance to inflowing rivers and local lake depth). This model enabled us to assess the relative importance of these factors contributing to lake water quality patterns and their interactions.

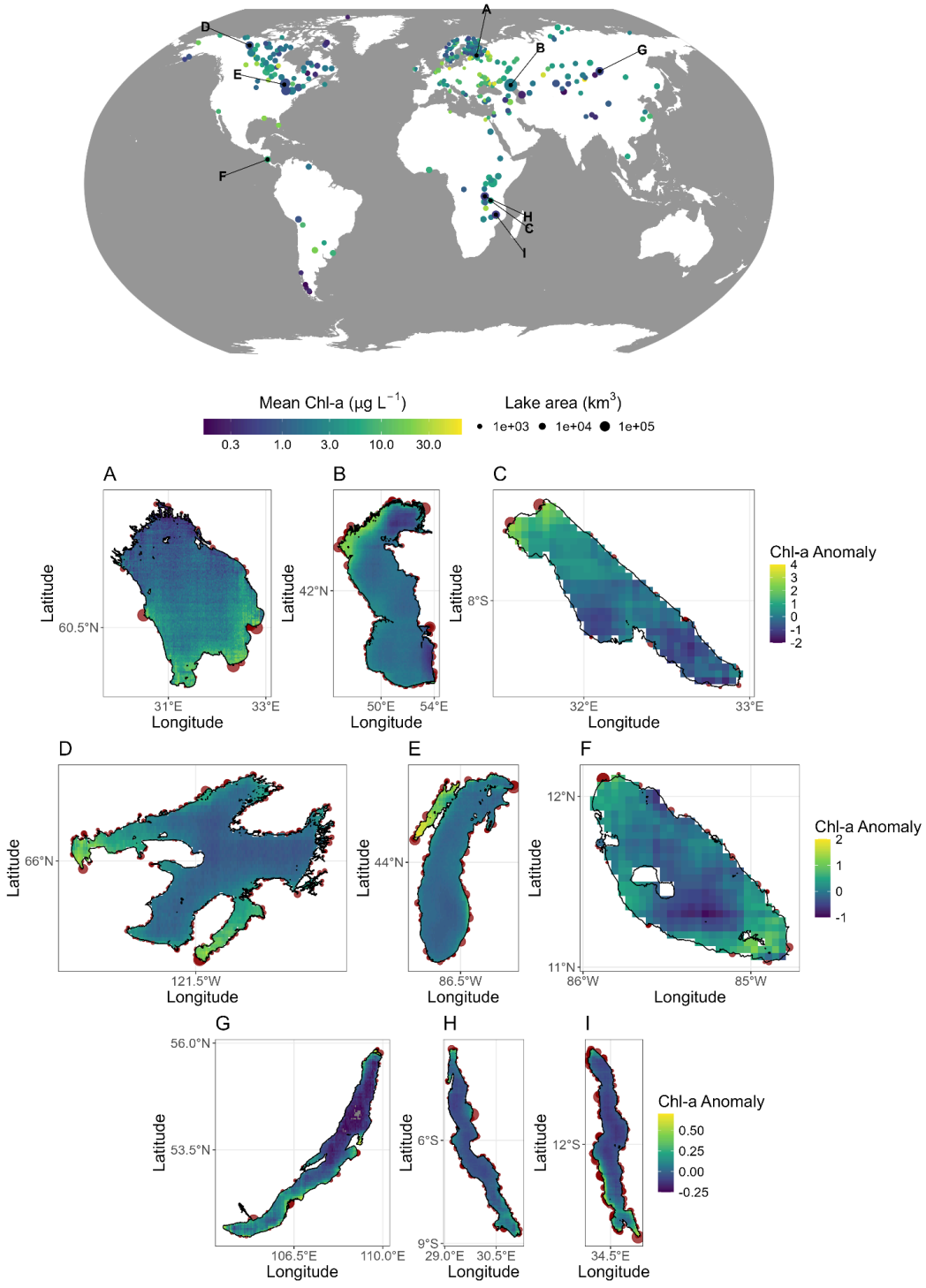

Figure 1 | Variation in chl-a across and within lakes with inlet locations scaled to discharge. Top panel shows a global map with the mean chlorophyll-a concentrations across major lakes. The size of each lake marker is proportional to lake surface area, and the color represents the mean chlorophyll-a concentration from 1997-2020. Several lakes are labeled with corresponding zoomed-in panels shown below (A: Ladoga, B: Caspian, C: Rukwa, D: Great Bear, E: Michigan, F: Nicaragua, G: Baikal, H: Tanganyika, I: Malawi). The anomaly represents

deviations from the lake-wide mean. Inlet locations are indicated with red points, and their sizes are scaled according to accumulated inflow. Black polygons in panels A-I show the lake boundaries and are sourced from HydroLAKES [11]. The color scale for chlorophyll-a anomaly in each row is adjusted based on the range of anomalies within the corresponding lakes. Legends for each row are placed on the right-hand side, showing chlorophyll-a anomaly from negative to positive values. The continent boundary map data comes from Natural Earth Data (http://www.naturalearthdata.com/about/terms-of-use/; public domain).

Across the globe, a combination of human land use, watershed climate and geography, and local characteristics explained 71% of the variation in chlorophyll-a concentrations. Among these factors, croplands were the most important driver of surface lake water quality, accounting for 18% of the explained variation (Fig. 2; Fig. S1). Specifically, chlorophyll-a concentrations more than tripled (from 1.9 to 6.0 μg L^{-1}) as the percentage of croplands in a watershed rose from 0% to 30% (Fig. 2A). However, at the higher end of the cropland gradient, chlorophyll-a became less sensitive to further changes—a plateauing effect that suggests additional increases in cropland have minimal impact on chlorophyll-a levels. This pattern may reflect a similar plateau in the relationship between agricultural coverage and fertilizer application, where total fertilizer use also does not increase substantially beyond 30% cropland coverage (Fig. S2). Furthermore, the effect of cropland extent in a lake's watershed depended strongly on the distance of sampling locations from inflowing rivers, shaping within-lake variations in chlorophyll-a. In fact, distance to inflowing rivers was the second most important variable in the boosted regression tree model, with a relative importance of 17% (Fig. S1). Chlorophyll-a concentrations decreased by 76% as the distance from inflowing rivers increased across the entire range of the predictor variable (Fig. 2B). High groundwater levels may exert a similar effect (Fig. S3), particularly in lowland river deltas and wetlands where shallow groundwater tables enhance nutrient connectivity to lakes. The interaction between these variables highlights that the combination of high cropland coverage and proximity to large inflowing rivers exerts a potent influence on chlorophyll-a concentrations (Fig. 2C).

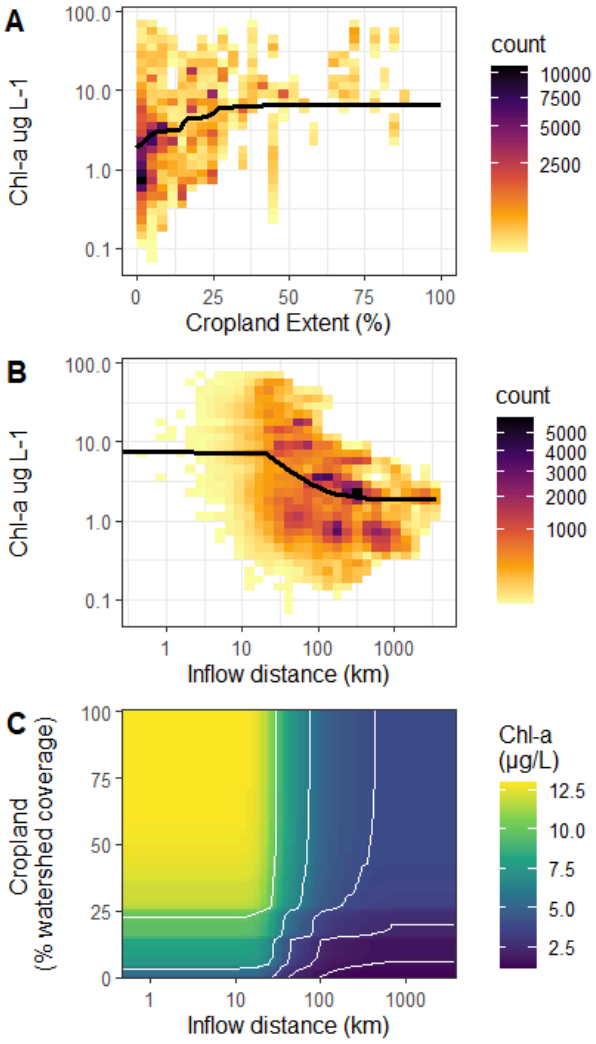

Figure 2 | Most influential drivers of lake chlorophyll-a concentrations. (A) The relationship between cropland extent and chlorophyll-a concentrations, where increased cropland coverage is associated with higher chlorophyll-a levels, as indicated by a fitted line (black) based on model predictions. Panel (B) depicts the relationship between inflow distance and chlorophyll-a concentrations, showing a trend of decreasing chlorophyll-a with increasing distance from inflows. Raw chl-a observations in (A) and (B) are depicted in the datacloud. Panel (C) combines cropland extent and inflow distance to show their interactive effects on chlorophyll-a concentrations. The color gradient indicates chlorophyll-a concentrations, with overlaid white contour lines representing concentration gradients on a log scale. Together, these plots highlight the significant influence of both agricultural land use and inflowing water on lake chl-a.

Global patterns reveal striking latitudinal differences in how effectively chlorophyll-a concentrations can be reduced by limiting nutrient pollution from human activities (Fig. 3). When nutrient inputs from croplands were reduced—modeled here as the equivalent of a 20%

decrease in cropland extent within each lake's watershed—the strongest responses often occurred between 30°S and 30°N. In this low-latitude band–encompassing many tropical lakes in regions such as East Africa, Southeast Asia, and northern South America–many tropical lakes exhibited some of the largest absolute and percentage reductions in surface chl-a concentrations. However, considerable variation exists within this tropical zone. Some latitudinal bins showed dramatic improvements, while others responded weakly, likely due to differences in baseline chl-a levels or cropland coverage (Fig. 3B, D). Notably, areas around 40°N, including parts of North America, southern Europe, and East Asia, displayed relatively small absolute declines but large proportional improvements—a pattern consistent with low baseline chl-a, where even modest pollution reductions can yield outsized effects. In contrast, mid-latitude regions (~50°–60°N), such as Canada, northern Europe, and parts of Russia, often showed larger absolute reductions, driven by high initial nutrient loads from intensive agriculture, but smaller proportional improvements. This reflects the plateauing effect described earlier: once cropland extent exceeds a certain threshold, further increases (or decreases) have diminishing influence on lake chl-a concentrations. Overall, while the biggest absolute improvements may occur in moderately impacted lakes below the plateau (e.g., <30% cropland coverage), the greatest proportional benefits can be achieved in less-impacted lakes, where cropland-derived nutrients disproportionately drive water quality degradation.

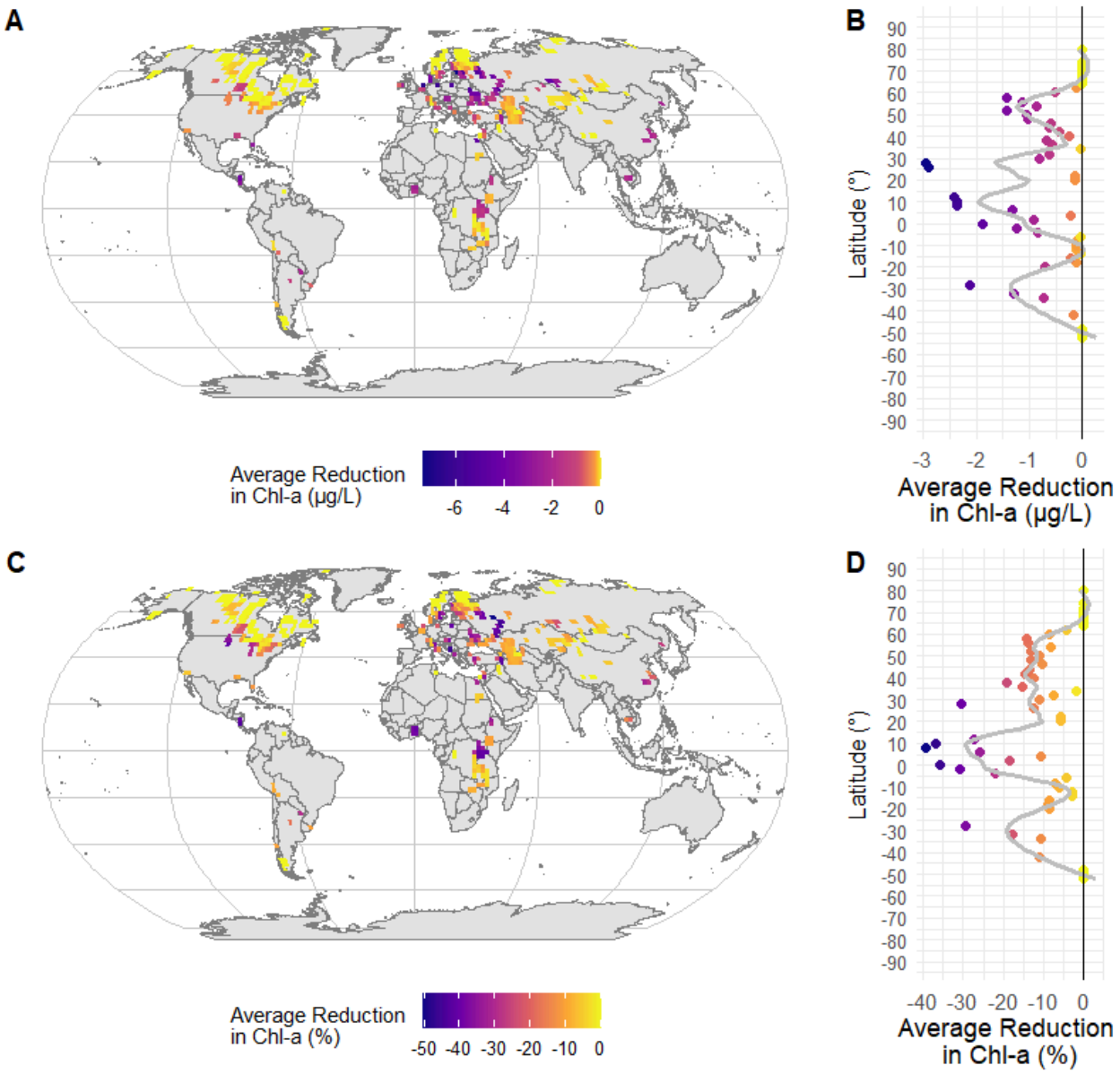

Fig 3: Global consequences of reduced cropland pollution on lake chl-a. Spatial and latitudinal patterns of differences in chlorophyll-a (chl-a) concentrations resulting from 20% lower nutrient pollution from croplands within lake watersheds. **(A)** Map of the absolute change in chl-a (µg/L) aggregated to 2-degree bins and projected using the Robinson projection. Each colored polygon represents the average reduction within a 2-degree grid cell, with lighter colors indicating smaller reductions and darker colors indicating larger reductions. **(B)** Vertical plot of the latitudinal averages of absolute change in chl-a across 2-degree bins, with a LOESS smoothed line to highlight the dominant latitudinal patterns. **(C)** Map of the percent reduction in chl-a, aggregated and displayed similarly to panel (A), but showing proportional changes. **(D)** Vertical plot of the latitudinal averages of percent reductions in chl-a, with magnitudes highlighted by LOESS smoothing. The maps and plots together illustrate both the magnitude and spatial variability of chl-a reductions, highlighting regions most sensitive to cropland extent

changes. Continent boundary map data come from Natural Earth. (http://www.naturalearthdata.com/about/terms-of-use/; public domain).

Interventions targeting different human activities vary widely in how effectively they reduce lake chl-a concentrations (Fig. 4). Among all drivers examined, reducing nutrient pollution from croplands had the largest global impact—lowering mean lake chl-a by up to ~1.9 µg/L and achieving proportional reductions of up to 31% when modeled at full (100%) reduction. By comparison, changes to other variables—such as sewage inputs (represented by population count) (Fig. S4), urban runoff (Fig. S5), Human Development Index (HDI) (Fig. S6), wetland coverage (Fig. S7), pastureland extent (Fig. S8), —produced more modest improvements in water quality. Improving sewage nutrient management alone could still reduce chl-a concentrations by up to 40% in some watersheds, particularly where agricultural impacts are minimal but population pressures are high. Interventions like expanding wetlands or raising HDI had more limited effects when considered in isolation. Even so, these variables offer indirect benefits that extend beyond chl-a reduction. Wetland restoration, for example, can improve wildlife habitat and trap sediments[12], while higher HDI levels are often associated with better environmental governance and infrastructure[13]. Groundwater management, however, presents a more complex picture: while deep groundwater levels can help reduce nutrient transport to lakes, overabstraction may offset such benefits[14]. Conversely, shallow groundwater tables, particularly in wetlands and deltas, can enhance nutrient connectivity and thus amplify eutrophication pressures[14]. These findings highlight the importance of combining strategies to enhance water quality through multiple co-benefits rather than relying on single interventions alone[15].

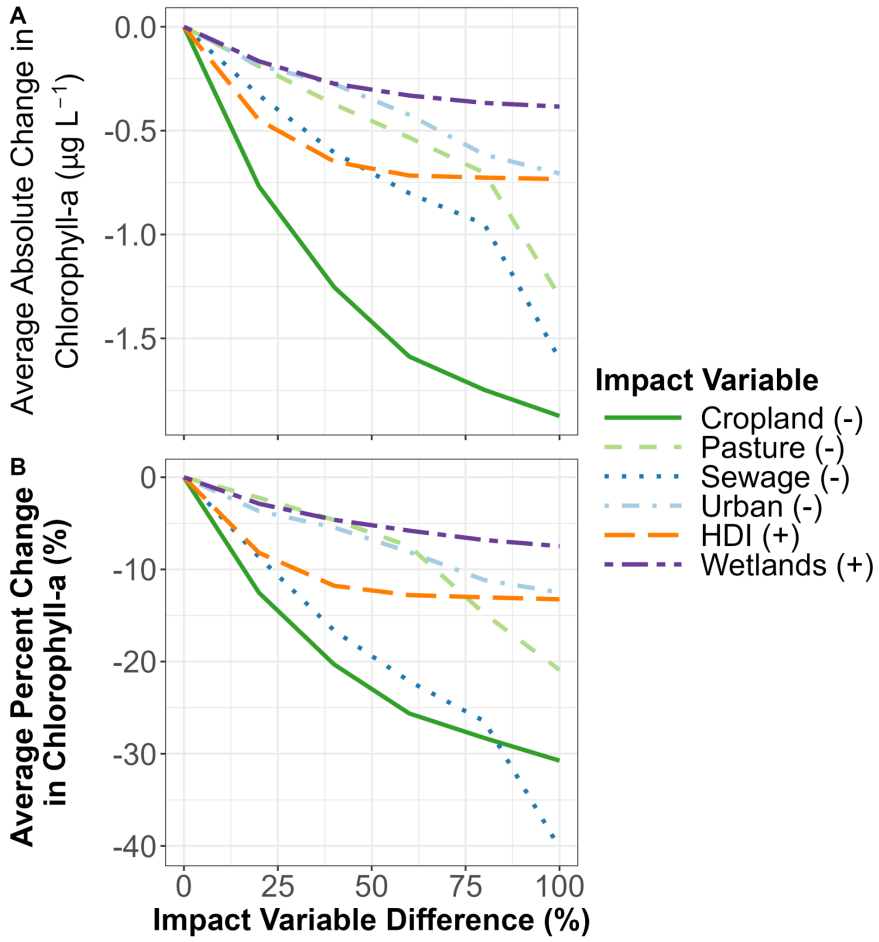

Fig. 4: Impact of human-driven environmental changes on average chlorophyll-a (chl-a) concentrations in freshwater systems. (A) Absolute change in chl-a (µg/L) as a function of differences in human impact variables as a percent difference (0 to 100%) from the present, averaged globally. (B) Percent change in chl-a as a function of the same reductions. Lines represent six key human impact variables. Reductions are applied incrementally, with absolute and percent changes modeled using boosted regression trees. The sign (+/-) indicates whether the modeled land-use change increases or decreases chl-a concentrations, respectively. These results highlight the differential sensitivity of freshwater chl-a concentrations to distinct human impact drivers.The relationship between modified global land use change (0 to 100%) and the resulting change in global average chl-a.

Interventions targeting nutrient pollution from land-use changes exhibit distinctly localized effects on chlorophyll-a (chl-a) concentrations in freshwater systems (Fig. 5). Reductions in cropland-derived nutrients, for example, could result in substantial decreases in chl-a concentrations near river inlets, but these benefits diminish rapidly with increasing distance offshore. This spatial limitation indicates that interventions targeting agricultural runoff

may primarily enhance nearshore water quality—an important outcome, as nearshore habitats typically support greater biodiversity and provide essential ecosystem services . Interestingly, the effectiveness of land-use changes varies considerably among the different impact variables examined. This variation may reflect differences in the type of nutrients and other biogeochemical constituents supplied by each source, as well as differences in their transport mechanisms. For instance, certain nutrients associated with pasture runoff might bind readily to sediments, limiting their offshore transport [16], whereas nutrients from urban runoff or sewage could remain dissolved longer and thus be carried farther offshore during intense rainfall events [17]. Such hydrological differences could partially explain why certain interventions yield greater offshore impacts than others. However, these hypotheses remain speculative and highlight the need for further investigation. Ultimately, while targeted land-use interventions provide valuable nearshore improvements, complementary strategies addressing offshore climate-related impacts will be necessary for comprehensive water-quality management in the context of global environmental change.

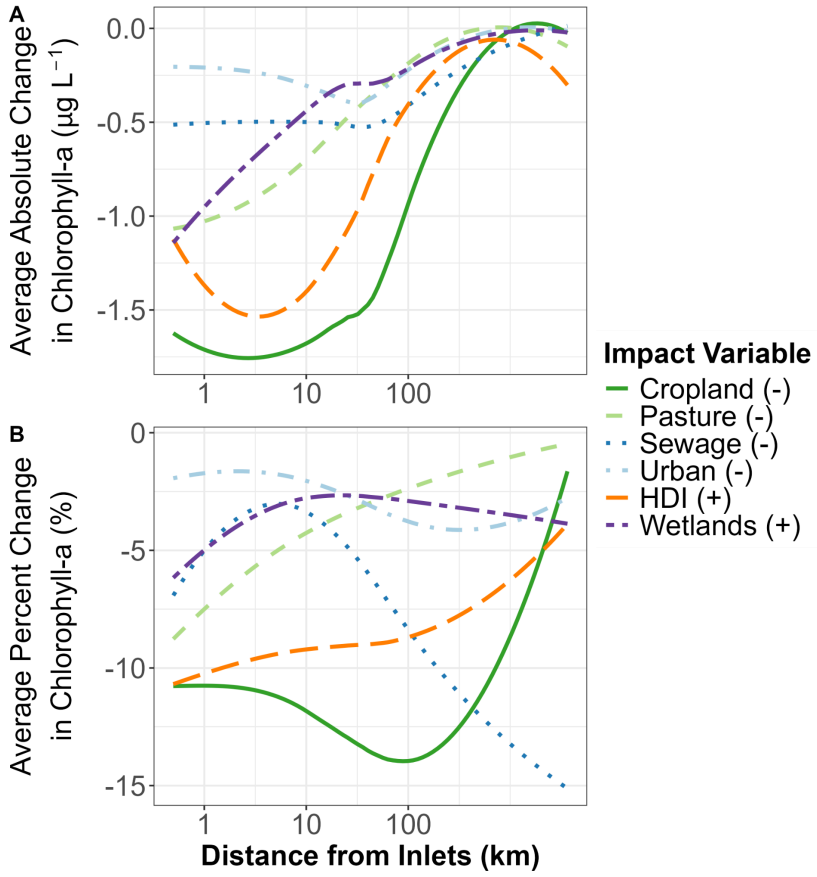

Figure 5: Localized impacts of land-use changes on chlorophyll-a concentrations. Modeled changes in chlorophyll-a (chl-a) concentrations resulting from a 20% change in land-use variables, plotted as a function of distance from river inlets. (A) Absolute change in chl-a (µg/L) shows limited response to land-use changes as the distance from inlets increases. (B) Percent change in chl-a highlights a similar trend, with diminished influence of land-use changes offshore. Six key variables are analyzed: cropland extent (green), pasture extent (light green), sewage (blue; approximated by population count), urban extent (light blue), human development index (orange), and wetland extent (purple). The sign (+/-) indicates whether the modeled land-use change increases or decreases chl-a concentrations, respectively. These results underscore the localized nature of land-use impacts on chl-a concentrations in freshwater systems.

Lakes across the globe are experiencing widespread water quality degradation, with agricultural nutrient pollution emerging as a dominant and spatially uneven driver. This degradation not only promotes excessive phytoplankton growth but also alters habitat conditions, reduces oxygen availability, and disrupts the ecological integrity of freshwater ecosystems. Although the basic mechanisms of eutrophication are well established, the spatial heterogeneity of its drivers—both within lakes and across global landscapes—could be better

understood. Our findings demonstrate that agricultural land use near major river inflows consistently elevated surface chlorophyll-a (chl-a) concentrations in the nearshore zones of lakes, where biodiversity and human use values tend to be highest. Simultaneously, the strength of this relationship varies systematically across regions, with lower-latitude lakes showing disproportionately large reductions in chl-a when agricultural nutrient pollution is curtailed. These results reveal a spatial mismatch between where degradation is concentrated and where monitoring and management efforts have traditionally focused—often in offshore, temperate-zone waters. Addressing this mismatch requires aligning observation and intervention strategies with the spatial scale at which degradation occurs, both within and among lakes, to effectively prioritize and tailor nutrient pollution mitigation efforts on a global scale.

Our results point to clear geographic opportunities for action. Among potential interventions, reducing agricultural nutrient inputs remains the most tractable and globally impactful strategy. Although agricultural eutrophication is often framed as a mid-latitude problem [3,18,19]—and undertreated sewage inputs as the dominant concern in lower latitudes [20,21]—our analysis challenges this dichotomy. We show that the largest proportional improvements in lake water quality from agricultural nutrient reductions are actually achievable in low-latitude regions, particularly in parts of Africa, Asia, and South America. This finding underscores the urgency of re-evaluating global nutrient management priorities, especially in regions where agricultural expansion is accelerating and wastewater infrastructure remains limited. Historically, point-source pollution was the primary driver of eutrophication in European lakes during the mid-20th century, with diffuse nutrient inputs from agriculture becoming more prominent only after substantial investments in sewage treatment [22]. In contrast, many industrializing regions now face both challenges simultaneously [23,24]—widespread agricultural runoff and insufficient wastewater treatment—highlighting the need for integrated strategies that address both point and nonpoint sources in tandem.

This study does not explicitly model the effects of climate change or its interactions with land use, focusing instead on spatial patterns of chlorophyll-a concentrations and their relationships to human activity. However, the processes identified here—particularly those concentrated near inflow regions—are likely to be highly sensitive to future climatic shifts [25,26]. For example, increased rainfall intensity, snowmelt, and extreme weather events driven by climate change are expected to intensify erosion and sediment mobilization in upstream catchments, delivering larger pulses of dissolved and particulate nutrients to lakes [27,28]. These hydrological disturbances can reinforce internal nutrient cycling [29,30] and establish positive

feedback loops that further elevate chl-a concentrations, especially in lakes already primed by river damming and channelization [25,30]. Moreover, climate change may alter agricultural practices themselves, potentially leading to increased fertilizer use or shifts in crop types that exacerbate nutrient runoff. While temperature emerged as a key predictor of spatial chl-a patterns in our model, it should not be interpreted as a temporal proxy for climate warming — substituting spatial gradients for climate trajectories in this case may be methodologically imprudent. Nonetheless, the mechanisms we document are likely to amplify under a warming climate, with implications not only for water quality but also for greenhouse gas emissions from lakes, as elevated chl-a is often linked to increased carbon and methane release [31]. These climate–land use–lake feedbacks remain poorly quantified at global scales and demand integrated investigation to anticipate future trajectories of freshwater degradation and carbon cycling. In addition, our analysis uses % cropland as a static variable representing long-term land-use intensity, yet cropland extent has changed substantially over recent decades. Between 1995 and 2020, agricultural expansion was especially pronounced in many low-latitude regions of Africa, Asia, and South America, whereas higher-latitude regions primarily intensified production through increased inputs rather than expanded area [32,33]. These contrasting trends suggest that future models incorporating time-varying land-use data could further clarify regional trajectories of nutrient pressures on lakes.

Efforts to reduce lake surface chlorophyll-a concentrations through land-use interventions will be ineffective if they are economically burdensome or lack social and political support. Even when grounded in strong scientific evidence, strategies such as reducing cropland extent or upgrading wastewater infrastructure will fail without broad acceptance among local communities, policymakers, and land managers. The social acceptability and cost-effectiveness of interventions vary widely: fertilizer regulations, for example, may be relatively inexpensive to implement but politically contentious, while infrastructure investments such as wastewater treatment upgrades demand substantial upfront resources. Moreover, economic pressures may incentivize short-term fixes over sustained, long-term strategies that offer broader water quality and climate co-benefits. Attitudes toward environmental action also diverge globally, shaped by governance capacity, development priorities, and cultural perceptions of responsibility. In some settings, stakeholders may favor local adaptation measures—such as hypolimnetic oxygenation or wetland restoration—that offer direct, visible benefits, even if these do little to reduce broader watershed-scale nutrient loading. Understanding the economic and sociopolitical constraints that shape intervention feasibility is therefore as essential as quantifying their biophysical impacts of water quality interventions.

Our global assessment shows that nutrient inputs from agriculture near river inflows are a pervasive and often decisive influence on lake eutrophication. Yet this pattern is far from uniform. In many tropical and subtropical regions, where cropland expansion continues alongside rapid population growth, lakes appear especially sensitive to agricultural pressures. Reducing the nutrient footprint of croplands—whether through smaller cultivated areas or improved nutrient-use efficiency—could yield the largest water-quality gains in these regions. However, such reductions are unlikely to be straightforward. Efforts to limit cropland expansion must contend with rising food demand, and intensification on existing farmland risks further nutrient leakage if fertilizer use increases unchecked. Moreover, the nearshore zones most affected by these inputs are rarely the focus of long-term monitoring, which means degradation is often underestimated. Addressing these challenges will require spatially targeted approaches that combine agricultural reform with improved wastewater treatment, particularly in rapidly urbanizing watersheds. Ultimately, equitable lake conservation depends on reconciling land-use efficiency with social and hydrological realities—ensuring that interventions are both regionally relevant and proportionate to the sources of degradation they aim to mitigate.

Methods:

Overview:

Here we used a large dataset of chlorophyll-a (chl-a) estimates to assess drivers in chl-a variation across and within 321 large lakes. We began by retrieving high-quality chl-a values, focusing on ice-free and cloud-free conditions, and further calibrated these data with in situ measurements to enhance the accuracy of remote sensing estimates specifically for each lake. Boosted Regression Trees (BRTs) were employed to model the relationship between chl-a concentrations and various environmental predictors, including human influence, climate, and lake characteristics. BRT was used because it can handle different data types, missing values, outliers, and the interaction effects between predictors, which is very useful in fitting complex nonlinear relationships [34]. Additionally, we examined spatial variation in chl-a within lakes by considering proximity to inlets and local depth, using weighted cost-distance metrics to capture nutrient dynamics. Finally, BRT models were also used to explore latitudinal trends and simulate land-use change impacts on lake chl-a.

Chl-a data:

We used 742 million chl-a estimates (after excluding ~76% of lower-quality observations due to partial cloud or ice cover) merged across 6 space-borne spectroradiometers (SeaWiFS, MODIS AQUA, MERIS, OLCI-B, VIIRS NPP, and VIIRS JPSS-1) to assess long-term trends in 321 lakes under ice-free and cloud-free conditions from year 1997 to 2020. Chl-a data were retrieved from the "CHL-OC5" product produced by GlobColour [35] and made available via the Copernicus Marine Environmental Monitoring Service (CMEMS) website: http://marine.copernicuseu/services-portfolio/access-to-products/. Only the highest-quality chl-a values (levels 4-5) were used according to the quality criteria provided as part of the CHL-OC5 data product. The algorithm used in the CHL-OC5 data product is a five-channel chlorophyll concentration algorithm which was developed for optically complex "case II waters" [36] and has been validated using global in situ data from marine and inland waters [6,37–40]. The daily chl-a data reflect lake environments in the near surface layer during ice-free and cloud-free conditions. The seasonal extent and the number of chl-a estimates varied across lakes ranging from 2601 estimates for Lake Mogotoyeyo to 365 million for Lake Ladoga. We downloaded and processed the chl-a values in the R environment for statistical computing [41] using the "data.table" [42], "dismo" [43], "sf"[44,45] [44], "gbm" [46], "zyp" [47] and "lubridate" [48] packages. Data visualizations were made using "ggplot2", [49] and "cowplot" [50].

Chl-a algorithm cross validation and calibration for inland waters:

We adapted remotely sensed chlorophyll-a (chl-a) values for lakes using 20,165 in situ chl-a measurements from 56 lakes, matched with interpolated remote sensing data [6]. For interpolation, we used deterministic boosted regression trees (BRTs) (bag fraction = 1) to model remotely sensed chl-a as a function of decimal date, day of the year, sensor, latitude, and longitude for each lake separately. These models estimated remotely sensed chl-a concentrations for six sensors at the time and location of each in situ measurement, creating remotely sensed matchup values. The in situ data had a mean chl-a of 8.7 μg L^{-1}, median chl-a of 3.9 μg L^{-1}, and a range from 0.01 to 579.2 μg L^{-1} (S2 Table). We would expect the calibrated chl-a algorithm used here to be less accurate near the tails and outside of the in situ chl-a distribution.

We modeled the difference between in situ and remotely sensed values as a function of raw remotely sensed chl-a, in situ data source, and three lake characteristics (mean lake depth, surface area, and shoreline development index) using a BRT. These characteristics are associated with lake optical properties and are freely available from the HydroLAKES database

[51]. The BRT allowed the difference between in situ and remotely sensed chl-a values to vary across lakes. We used the resulting model to estimate the difference for all 742 million chl-a estimates. Remotely sensed chl-a values were translated into “in situ analogue” chl-a values by subtracting the modeled differences from the raw values. This calibration reduced the median absolute error from 3.6 μg L^{-1} to 1.5 μg L^{-1} [6].

Predictors of chl-a:

We modeled within- and across-lake variation in average chlorophyll-a concentrations using 15 environmental predictors grouped into three categories: watershed human influence, watershed climate and geography, and within-lake location. The model selection approach prioritized variables based on their raw correlations with chlorophyll-a (chl-a), beginning with hypothesized key drivers and iteratively adding additional predictors while controlling for multicollinearity. Predictors hypothesized to directly influence chl-a were included first and allowed to have pairwise correlations among themselves of up to 0.7 following established criteria [52] (Fig. S10). Substitutions were made where necessary to meet the 0.7 correlation threshold, such as using urban area within 3 km of the lake instead of human population count to reduce collinearity with watershed population count. After hypothesized drivers were included, additional predictors were selected iteratively based on their raw correlations with chl-a, with pairwise correlations among already-selected predictors restricted to 0.35 to minimize redundancy with hypothesized drivers. To improve normality and interpretability of continuous predictors, we applied a systematic approach to identify appropriate transformations. For each variable, we assessed normality using the Shapiro-Wilk test for small-to-moderate sample sizes or the Anderson-Darling test for larger datasets. Variables that did not meet normality ($p < 0.05$) were transformed based on their skewness: log transformation was applied for strong positive skew, square root transformation for moderate positive skew, and square transformation for strong negative skew.

These predictors represent critical drivers of lake conditions across human, climate, and spatial dimensions. The three categories of predictors included in the model are listed below. Original variable names from LakeATLAS are provided in parentheses following the standard name of each variable (e.g. “crp_pc_use”) along with an added suffix for the transformation that was applied (e.g. “_log”) prior to model fitting.

1) Watershed Human Influence

This category represents direct anthropogenic pressures on lake ecosystems, influencing nutrient and sediment inputs:

- Cropland extent (crp_pc_use_log): The log-transformed percentage of the watershed used for croplands [53].
- Pastureland extent (pst_pc_use_log): The log-transformed percentage of the watershed used for pasture [53].
- Population count (pop_ct_usu_log): The log-transformed total human population count in each lake's watershed [54].
- Urban extent (urb_pc_vse_log): The log-transformed percentage of urban area in a 3 km buffer area surrounding each lake [55].
- HDI (Index) (hdi_ix_vav_squared): The squared Human Development Index, serving as a socio-economic indicator. The Human Development Index (HDI) is a composite statistic used to rank countries based on human development levels. It comprises three key dimensions: life expectancy at birth, mean years of schooling combined with expected years of schooling, and gross national income per capita. Each dimension is normalized to a scale from 0 to 1, and the HDI is calculated as the geometric mean of these three normalized indices, providing a single value that reflects a country's average achievements in health, education, and income [56].

2) Watershed Climate and Geography

This category includes broader physical and climatic features of the watershed that shape lake hydrology and nutrient transport:

- Groundwater table within 3 km (gwt_cm_vav_log): The log-transformed depth to the groundwater table within 3 km of the lake [57].
- Temperature (tmp_dc_uyr_sqrt): The square-root-transformed annual mean air temperature [58].
- Elevation (ele_mt_uav_log): The log-transformed average elevation of the watershed, influencing regional climate and hydrological gradients [59].
- Wetland extent within 3 km (wet_pc_vg2_log): The log-transformed percentage of wetlands within 3 km of the lake, reflecting localized nutrient retention and sediment trapping [60].

- Wetland extent (wet_pc_ug2_log): The log-transformed percentage of wetlands in the entire watershed, providing a broader view of hydrological and ecological wetland influence [60].
- Silt extent (slt_pc_uav_sqrt): The square-root-transformed percentage of soil silt in the watershed [61].
- Karst extent (kar_pc_vse_log): The log-transformed percentage of the watershed characterized by karst geology, indicating regions prone to groundwater infiltration and nutrient transport pathways [62].
- Evapotranspiration (aet_mm_vyr_log): The log-transformed annual actual evapotranspiration, representing watershed-scale water balance dynamics [63].

3) Within-Lake Location

This category reflects spatial features and nutrient delivery within the lake system:

- Lake depth: The log-transformed depth of the lake, influencing nutrient recycling and stratification [64].
- Inflow distance: A log-transformed metric combining proximity to major inlets and their flow contributions, capturing spatial variability in the proximity to nutrient delivery from inflowing waters [51,64].

To assess the influence of lake inlets on spatial chlorophyll-a concentration patterns, we first identified the major inlets for each lake and calculated cost distances across the lake using bathymetric data [64]. For each lake, we extracted bathymetric raster data from a high-resolution bathymetry dataset, representing water depths within each lake. The locations and drainage accumulation values of inlets were extracted from HydroSHEDS [65]. We identified the largest inlets based on flow accumulation, filtering for inlets whose accumulation exceeded the mean accumulation value for that lake. This ensured that the analysis focused on major inlets that typically have the dominant influence on lake nutrient budgets [66]. We then calculated cost distances between all inlet locations and all lake chl-a pixels, where the cost function was inversely proportional to the cube root of the local depth, reflecting the assumption that greater depths dilute incoming nutrients. The cost distance between all inlets and lake chl-a pixels in the lake was computed using the geo-corrected transition matrix using the ‘gdistance’ package [67] in R. The cost distances were combined with inlet flow accumulation values to compute a weighted mean cost distance for each latitude-longitude point in the lake. This weighted

distance metric incorporated both geographic proximity to inlets and the magnitude of flow entering from the inlets, offering a spatially explicit metric of the influence of all inlets on lake conditions at each chl-a pixel within the lake (Fig. S11).

Model fitting:

We used BRTs to explain with- and across- lake variation in chl-a. We optimized the learning rate by iteratively running the model with smaller and smaller learning rates (from 0.8, 0.4, 0.2, 0.1, 0.05 to 0.025) until the number of trees in the model was greater than 1,000, as suggested in previous literature [34]. The BRT model uses a Gaussian error distribution, a tree complexity of 6, and a bag fraction of 0.1 to avoid model overfitting. The initial model was fitted without imposing monotonicity constraints. However, after examining the results, it became evident that all predictor variables exhibited clear monotonic trends. To reduce the potential for overfitting, we re-fitted the model with each predictor constrained to be either monotonic increasing or decreasing. This adjustment simplified the predictor-response relationships, reducing unnecessary complexity and ensuring more interpretable patterns.The BRT performed well in cross-validation: out-of-fold RMSE was 0.676 (95% CI: 0.672–0.681), the correlation between predictions and observations was 0.842 (95% CI: 0.840–0.845), and deviance was 0.457 (95% CI: 0.451–0.463). We found minimal patterning in the model residuals when comparing the model residuals with each predictor variable used in the BRT.

Latitudinal variation in the potential for reductions in lake chl-a by reducing human impact variables:

We simulated different scenarios of changes to human impact variables by systematically changing the values for those variables by specified percentages (25%, 50%, 75%, and 100%) and testing the effect on modelled chl-a across all lake gridcells. The effect of these reductions on chlorophyll-a concentrations was predicted using the fitted BRT model, and the absolute and percentage reduction in chlorophyll-a was calculated relative to the baseline observations. These results were aggregated into 2-degree latitude bins to analyze spatial patterns in chlorophyll-a reduction.

Code and Data Availability Statement: All code and data used in this manuscript are available for download at the following DOI: https://doi.org/10.5281/zenodo.17582203

References:

1. Jane, S. F. *et al.* Widespread deoxygenation of temperate lakes. *Nature* **594**, 66–70 (2021).
2. Wurtsbaugh, W. A., Paerl, H. W. & Dodds, W. K. Nutrients, eutrophication and harmful algal blooms along the freshwater to marine continuum. *WIREs Water* **6**, e1373 (2019).
3. Withers, P. J. A., Neal, C., Jarvie, H. P. & Doody, D. G. Agriculture and Eutrophication: Where Do We Go from Here? *Sustainability* **6**, 5853–5875 (2014).
4. Sharpley, A. N. *et al.* Managing Agricultural Phosphorus for Protection of Surface Waters: Issues and Options. *J. Environ. Qual.* **23**, 437–451 (1994).
5. Jenny, J.-P. *et al.* Urban point sources of nutrients were the leading cause for the historical spread of hypoxia across European lakes. *Proc. Natl. Acad. Sci.* **113**, 12655–12660 (2016).
6. Kraemer, B. M., Kakouei, K., Munteanu, C., Thayne, M. W. & Adrian, R. Worldwide moderate-resolution mapping of lake surface chl-a reveals variable responses to global change (1997–2020). *PLOS Water* **1**, e0000051 (2022).
7. Ho, J. C., Michalak, A. M. & Pahlevan, N. Widespread global increase in intense lake phytoplankton blooms since the 1980s. *Nature* **574**, 667–670 (2019).
8. Oliver, S. K. *et al.* Unexpected stasis in a changing world: Lake nutrient and chlorophyll trends since 1990. *Glob. Change Biol.* **23**, 5455–5467 (2017).
9. Wilkinson, G. M., Walter, J. A., Buelo, C. D. & Pace, M. L. No evidence of widespread algal bloom intensification in hundreds of lakes. *Front. Ecol. Environ.* **20**, 16–21 (2022).
10. Caron, D. A. *et al.* Macro- to fine-scale spatial and temporal distributions and dynamics of phytoplankton and their environmental driving forces in a small montane lake in southern California, USA. *Limnol. Oceanogr.* **53**, 2333–2349 (2008).
11. Mackay, E. B., Jones, I. D., Thackeray, S. J. & Folkard, A. M. Spatial heterogeneity in a small, temperate lake during archetypal weak forcing conditions. *Fundam. Appl. Limnol.* 27–40 (2011) doi:10.1127/1863-9135/2011/0179-0027.
12. Zedler, J. B. & Kercher, S. WETLAND RESOURCES: Status, Trends, Ecosystem Services,

and Restorability. *Annu. Rev. Environ. Resour.* **30**, 39–74 (2005).

13. Boretti, A. & Rosa, L. Reassessing the projections of the world water development report. *NPJ Clean Water* **2**, 15 (2019).
14. Van Loon, A. F. *et al.* Drought in a human-modified world: reframing drought definitions, understanding, and analysis approaches. *Hydrol. Earth Syst. Sci.* **20**, 3631–3650 (2016).
15. Downing, J. A., Polasky, S., Olmstead, S. M. & Newbold, S. C. Protecting local water quality has global benefits. *Nat. Commun.* **12**, 2709 (2021).
16. McDowell, R. & and Wilcock, R. Water quality and the effects of different pastoral animals. *N. Z. Vet. J.* **56**, 289–296 (2008).
17. Lintern, A. *et al.* Key factors influencing differences in stream water quality across space. *WIREs Water* **5**, e1260 (2018).
18. Smith, V. Eutrophication of freshwater and coastal marine ecosystems a global problem. *Environ. Sci. Pollut. Res.* **10**, 126–139 (2003).
19. Carpenter, S. R. *et al.* Nonpoint Pollution of Surface Waters with Phosphorus and Nitrogen. *Ecol. Appl.* **8**, 559–568 (1998).
20. Wear, S. L., Acuña, V., McDonald, R. & Font, C. Sewage pollution, declining ecosystem health, and cross-sector collaboration. *Biol. Conserv.* **255**, 109010 (2021).
21. Altieri, A. H. *et al.* Tropical dead zones and mass mortalities on coral reefs. *Proc. Natl. Acad. Sci.* **114**, 3660–3665 (2017).
22. Jeppesen, E. *et al.* Lake responses to reduced nutrient loading - An analysis of contemporary long-term data from 35 case studies. *Freshw. Biol.* **50**, 1747–1771 (2005).
23. Jiang, L. & O'Neill, B. C. Global urbanization projections for the Shared Socioeconomic Pathways. *Glob. Environ. Change* **42**, 193–199 (2017).
24. Zabel, F. *et al.* Global impacts of future cropland expansion and intensification on agricultural markets and biodiversity. *Nat. Commun.* **10**, 2844 (2019).
25. Carpenter, S. R. *et al.* Ecological and economic analysis of lake eutrophication by nonpoint

pollution. *Aust. J. Ecol.* **23**, 68–79 (1998).

26. Smith, V., Tilman, G. & Nekola, J. Eutrophication: impacts of excess nutrient inputs on freshwater, marine, and terrestrial ecosystems. *Environ. Pollut.* **100**, 179–196 (1999).
27. Walling, D. E. & Fang, D. Recent trends in the suspended sediment loads of the world's rivers. *Glob. Planet. Change* **39**, 111–126 (2003).
28. Withers, P. J. A. & Jarvie, H. P. Delivery and cycling of phosphorus in rivers: a review. *Sci. Total Environ.* **400**, 379–395 (2008).
29. Jeppesen, E. *et al.* Climate Change Effects on Runoff, Catchment Phosphorus Loading and Lake Ecological State, and Potential Adaptations. *J. Environ. Qual.* **38**, 1930–1941 (2009).
30. Maavara, T. *et al.* Global phosphorus retention by river damming. *Proc. Natl. Acad. Sci.* **112**, 15603–15608 (2015).
31. Yang, Y. *et al.* Climate change exacerbates the environmental impacts of agriculture. *Science* **385**, eadn3747 (2024).
32. Winkler, K., Fuchs, R., Rounsevell, M. & Herold, M. Six decades of global crop yield increase and cropland expansion from 1960 to 2020. *Environ. Res. Commun.* **7**, 055013 (2025).
33. Potapov, P. *et al.* Global maps of cropland extent and change show accelerated cropland expansion in the twenty-first century. *Nat. Food* **3**, 19–28 (2022).
34. Elith, J., Leathwick, J. & Hastie, T. A working guide to boosted regression trees. *J. Anim. Ecol.* **77**, 802–813 (2008).
35. Maritorena, S., d'Andon, O. H. F., Mangin, A. & Siegel, D. A. Merged satellite ocean color data products using a bio-optical model: Characteristics, benefits and issues. *Remote Sens. Environ.* **114**, 1791–1804 (2010).
36. Gohin, F., Druon, J. N. & Lampert, L. A five channel chlorophyll concentration algorithm applied to Sea WiFS data processed by SeaDAS in coastal waters. *Int. J. Remote Sens.* **23**, 1639–1661 (2002).

37. Gbagir, A.-M. G. & Colpaert, A. Assessing the Trend of the Trophic State of Lake Ladoga Based on Multi-Year (1997–2019) CMEMS GlobColour-Merged CHL-OC5 Satellite Observations. *Sensors* **20**, 6881 (2020).
38. Xi, H. *et al.* Global retrieval of phytoplankton functional types based on empirical orthogonal functions using CMEMS GlobColour merged products and further extension to OLCI data. *Remote Sens. Environ.* **240**, 111704 (2020).
39. Pitarch, J., Volpe, G., Colella, S., Krasemann, H. & Santoleri, R. Remote sensing of chlorophyll in the Baltic Sea at basin scale from 1997 to 2012 using merged multi-sensor data. *Ocean Sci.* **12**, 379–389 (2016).
40. Lavigne, H. *et al.* Quality-control tests for OC4, OC5 and NIR-red satellite chlorophyll-a algorithms applied to coastal waters. *Remote Sens. Environ.* **255**, 112237 (2021).
41. R Core Team. R: A Language and Environment for Statistical Computing. *R Foundation for Statistical Computing* R Foundation for Statistical Computing (2020).
42. Dowle, M. & Srinivasan, A. *Data.Table: Extension of `data.Frame`*. (2021).
43. Hijmans, R. J., Phillips, S., Leathwick, J., Elith, J. & Hijmans, M. R. J. Package 'dismo'. *Circles* **9**, 1–68 (2017).
44. Pebesma, E. J. Simple features for R: Standardized support for spatial vector data. *R J* **10**, 439 (2018).
45. Pebesma, E. & Bivand, R. *Spatial Data Science: With Applications in R*. (Chapman and Hall/CRC, 2023).
46. Greenwell, B., Boehmke, B., Cunningham, J., Developers, G. B. M. & Greenwell, M. B. Package 'gbm'. *R Package Version* **2**, (2019).
47. Bronaugh, D., Werner, A. & Bronaugh, M. D. Package 'zyp'. *CRAN Repos.* (2009).
48. Grolemund, G. & Wickham, H. Dates and times made easy with lubridate. *J. Stat. Softw.* **40**, 1–25 (2011).
49. Wickham, H., Chang, W. & Wickham, M. H. Package 'ggplot2'. *Create Elegant Data Vis.*

Using Gramm. Graph. Version **2**, 1–189 (2016).

50. Wilke, C. O. cowplot: Streamlined plot theme and plot annotations for'ggplot2'. *CRAN Contrib. Packag.* https://cir.nii.ac.jp/crid/1360582250132601088 (2015).
51. Lehner, B., Messager, M. L., Korver, M. C. & Linke, S. Global hydro-environmental lake characteristics at high spatial resolution. *Sci. Data* **9**, 1–19 (2022).
52. Dormann, C. F. *et al.* Collinearity: a review of methods to deal with it and a simulation study evaluating their performance. *Ecography* **36**, 27–46 (2013).
53. Farming the planet: 1. Geographic distribution of global agricultural lands in the year 2000 - Ramankutty - 2008 - Global Biogeochemical Cycles - Wiley Online Library. https://agupubs.onlinelibrary.wiley.com/doi/full/10.1029/2007GB002952.
54. Ciesin, I. Gridded population of the world, version 4 (gpwv4): population count. Palisades, NY: NASA socioeconomic data and applications center (SEDAC). *Cent. Int. Earth Sci. Inf. Netw. CIESIN Columbia Univ.* (2016).
55. Pesaresi, M. & Freire, S. GHS Settlement grid following the REGIO model 2014 in application to GHSL Landsat and CIESIN GPW v4-multitemporal (1975-1990-2000-2015). *JRC Data Cat* (2016).
56. Kummu, M., Taka, M. & Guillaume, J. H. A. Gridded global datasets for Gross Domestic Product and Human Development Index over 1990–2015. *Sci. Data* **5**, 180004 (2018).
57. Fan, Y., Li, H. & Miguez-Macho, G. Global Patterns of Groundwater Table Depth. *Science* **339**, 940–943 (2013).
58. Hijmans, R. J., Cameron, S. E., Parra, J. L., Jones, P. G. & Jarvis, A. Very high resolution interpolated climate surfaces for global land areas. *Int. J. Climatol. J. R. Meteorol. Soc.* **25**, 1965–1978 (2005).
59. Robinson, N., Regetz, J. & Guralnick, R. P. EarthEnv-DEM90: A nearly-global, void-free, multi-scale smoothed, 90m digital elevation model from fused ASTER and SRTM data. *ISPRS J. Photogramm. Remote Sens.* **87**, 57–67 (2014).

60. Lehner, B. & Döll, P. Development and validation of a global database of lakes, reservoirs and wetlands. *J. Hydrol.* **296**, 1–22 (2004).
61. Hengl, T. *et al.* SoilGrids1km—global soil information based on automated mapping. *PloS One* **9**, e105992 (2014).
62. Williams, P. W. & Ford, D. C. Global distribution of carbonate rocks. *Z. Geomorphol. Suppl.* **147**, 1 (2006).
63. Trabucco, A. & Zomer, R. J. Global soil water balance geospatial database. *CGIAR Consort. Spat. Inf.* (2010).
64. Khazaei, B., Read, L. K., Casali, M., Sampson, K. M. & Yates, D. N. GLOBathy, the global lakes bathymetry dataset. *Sci. Data* **9**, 36 (2022).
65. Lehner, B., Verdin, K. & Jarvis, A. New global hydrography derived from spaceborne elevation data. *Eos Trans. Am. Geophys. Union* **89**, 93–94 (2008).
66. Mooney, R. J. *et al.* Outsized nutrient contributions from small tributaries to a Great Lake. *Proc. Natl. Acad. Sci.* **117**, 28175–28182 (2020).
67. Etten, J. van, Sousa, K. de, Marx [cre, A. & ctb. gdistance: Distances and Routes on Geographical Grids. (2023).
68. Foley, J. A. *et al.* Global Consequences of Land Use. *Science* **309**, 570–574 (2005).
69. Potter, P., Ramankutty, N., Bennett, E. M. & Donner, S. D. Characterizing the spatial patterns of global fertilizer application and manure production. *Earth Interact.* **14**, 1–22 (2010).
70. Wood, S. & Wood, M. S. Package 'mgcv'. *R Package Version* **1**, 729 (2015).
71. Massicotte, P. & South, A. rnaturalearth: World map data from natural earth. *R Package Version 03* **2**, (2023).

Supplemental figures:

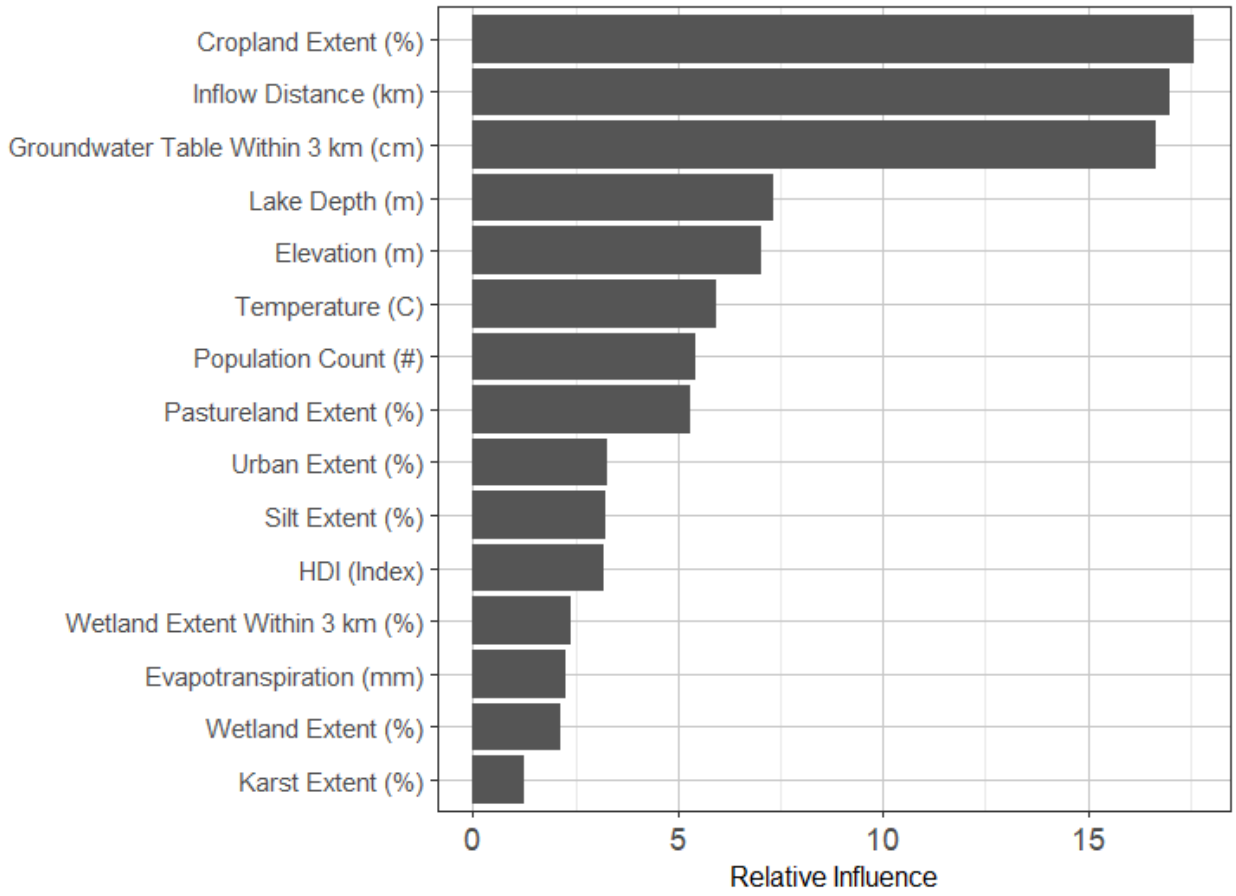

Figure S1 | Relative influence of predictors in boosted regression tree (BRT) analysis for lake chl-a. *Predictor variables are ranked by their relative influence (%) on the model, with cropland extent (%), inflow distance (km), and groundwater table depth (cm) identified as the strongest drivers. Variables include land use (e.g., urban, pasture, cropland), hydrological features (e.g., wetland extent, evapotranspiration), and lake characteristics (depth, elevation). All predictors were log- or square root-transformed for analysis. Axis labels reflect simplified, interpretable names for raw variables (e.g., "HDI (Index)" for Human Development Index). The BRT model was implemented in R using the dismo package, with relative influence calculated from 15 predictors.*

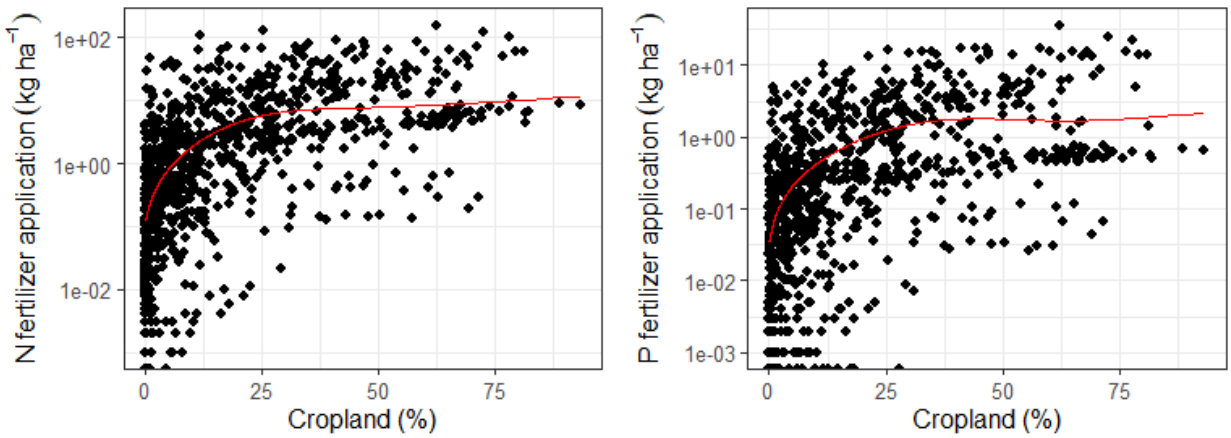

Figure S2 | Relationship between cropland percent coverage and N and P fertilizer application rates for the locations of lake inlets. *Nitrogen (N) and phosphorus (P) fertilizer application rates (kg ha⁻¹, log-transformed y-axes) are plotted against cropland cover (%) for upstream watersheds. Red lines represent generalized additive model (GAM) predictions using smoothing splines, with N and P values log-transformed to approximate normality. Observed data (points) show variability in fertilizer inputs across cropland gradients. Non-linear trends suggest increasing N and P application rates with cropland expansion, though the relationship plateaus at higher cropland percentages (>70%). Data were sourced from watershed-scale agricultural inventories, with cropland cover derived from land use datasets [68] and fertilizer rates estimated from farm surveys [69]. Models were fit in R using the 'mgcv' package [70].*

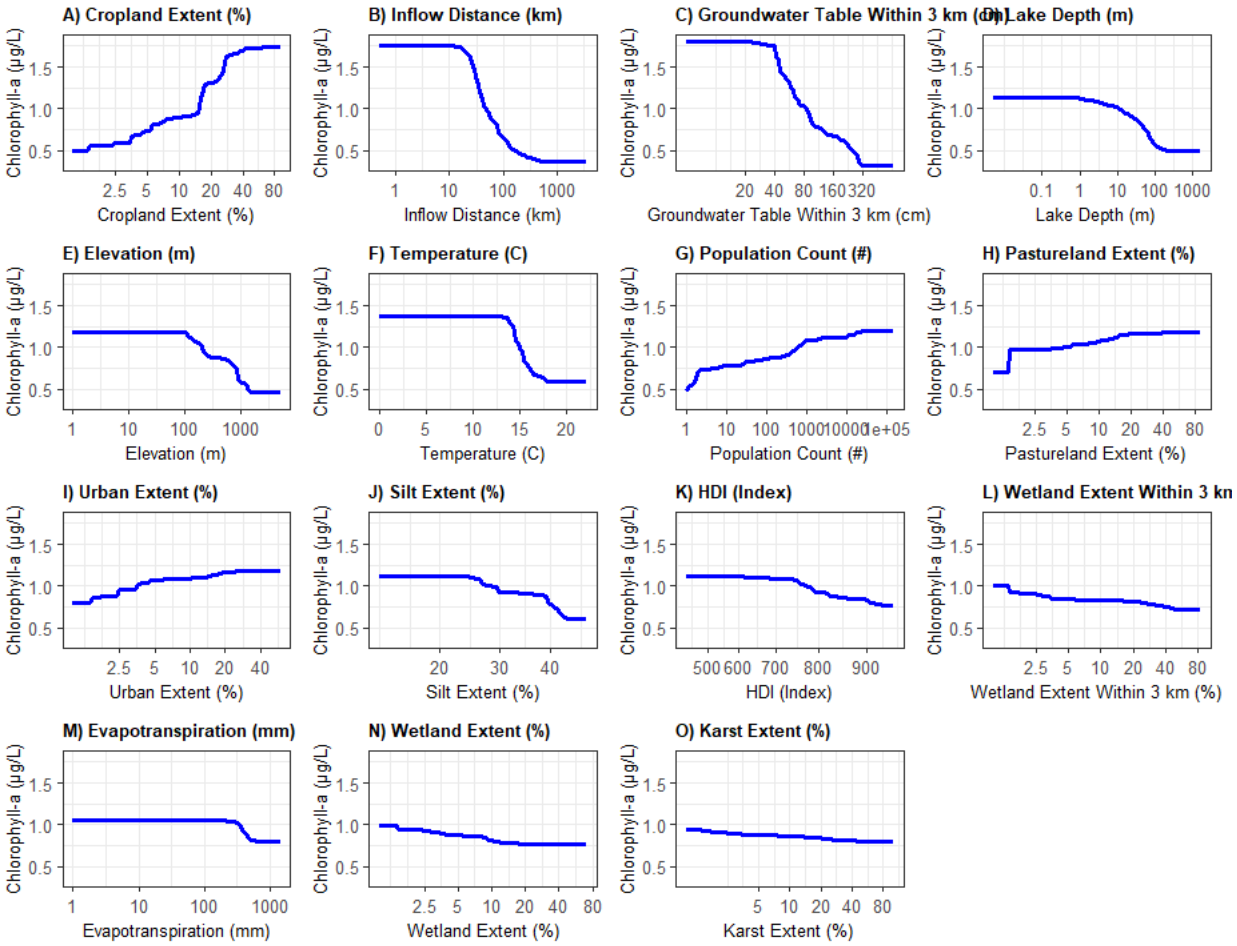

Figure S3 | Partial dependence relationships between predictors and chlorophyll-a concentrations in lakes. *Chlorophyll-a (µg/L, response variable) is modeled as a function of 15 predictors using a boosted regression tree (BRT). Each panel (A–O) shows the marginal effect of a transformed predictor (log- or square root-scaled) on chlorophyll-a, with predictors including cropland extent (%), groundwater table depth (cm), urban land cover (%), and lake depth (m). Non-linear relationships are shown as blue lines, with y-axis bounds fixed globally (range: [min, max] µg/L) to enable cross-panel comparison. Partial dependence values were computed using the gbm package in R, with predictor effects isolated while holding other variables at their means. Letters (A–O) in panel corners correspond to variable order in supplementary tables. Predictor labels reflect simplified names (e.g., "HDI (Index)" for Human Development Index). Data were derived from geospatial, hydrological, and socioeconomic datasets. Plots were generated in R using ggplot2* [49]*, with gridlines and consistent theming for clarity.*

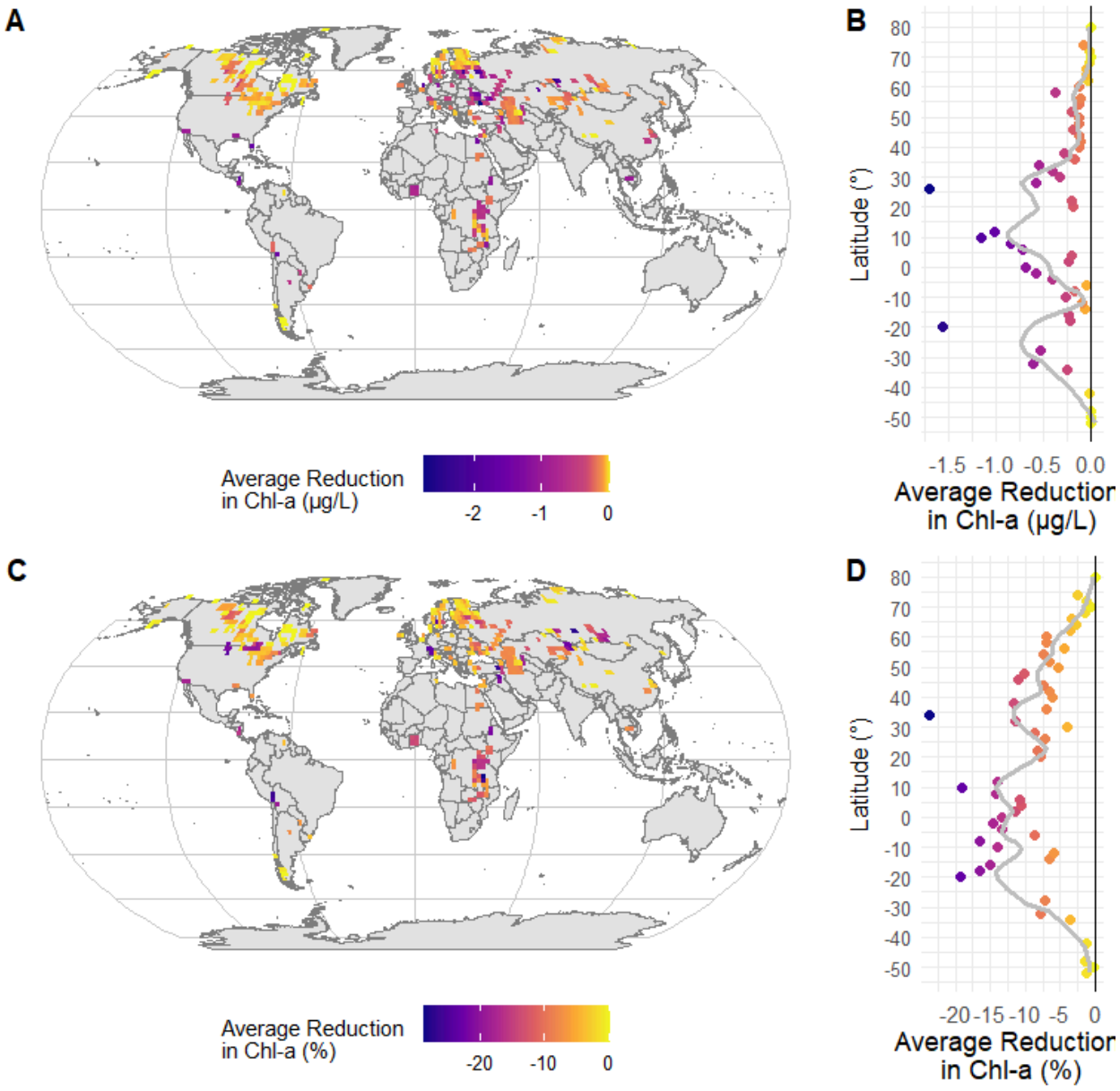

Figure S4 | Global latitudinal patterns of chlorophyll-a (chl-a) reduction associated with a 20% reduction in sewage pollution, assuming a linear relationship between human population size and sewage outputs. *(A) Global distribution of absolute chl-a reduction (µg/L) aggregated in 2° latitude-longitude bins, displayed in Robinson projection. (B) Latitudinal trends in absolute chl-a reduction, with a LOESS-smoothed line (span = 0.25) highlighting median changes. (C) Percent reduction in chl-a, similarly binned and projected. (D) Corresponding latitudinal trends for percent change. Data represent estimates based on aggregated global population count records, with reductions calculated as the mean change per bin. Human population size and associated sewage outputs correlate with greater chl-a reductions in densely populated mid-latitude regions (30°–50°), particularly in the Northern Hemisphere. Gray*

shading in maps represents landmasses; missing data indicate sparse sampling in polar and remote regions. Spatial aggregation and analysis performed in R using "sf"[44,45] and "ggplot2"[49] packages. Gray basemaps are from Natural Earth[71]. Watershed human population data from LakeAtlas.[51] Bias-corrected lake chl-a data from Kraemer et al. (2022)[6].

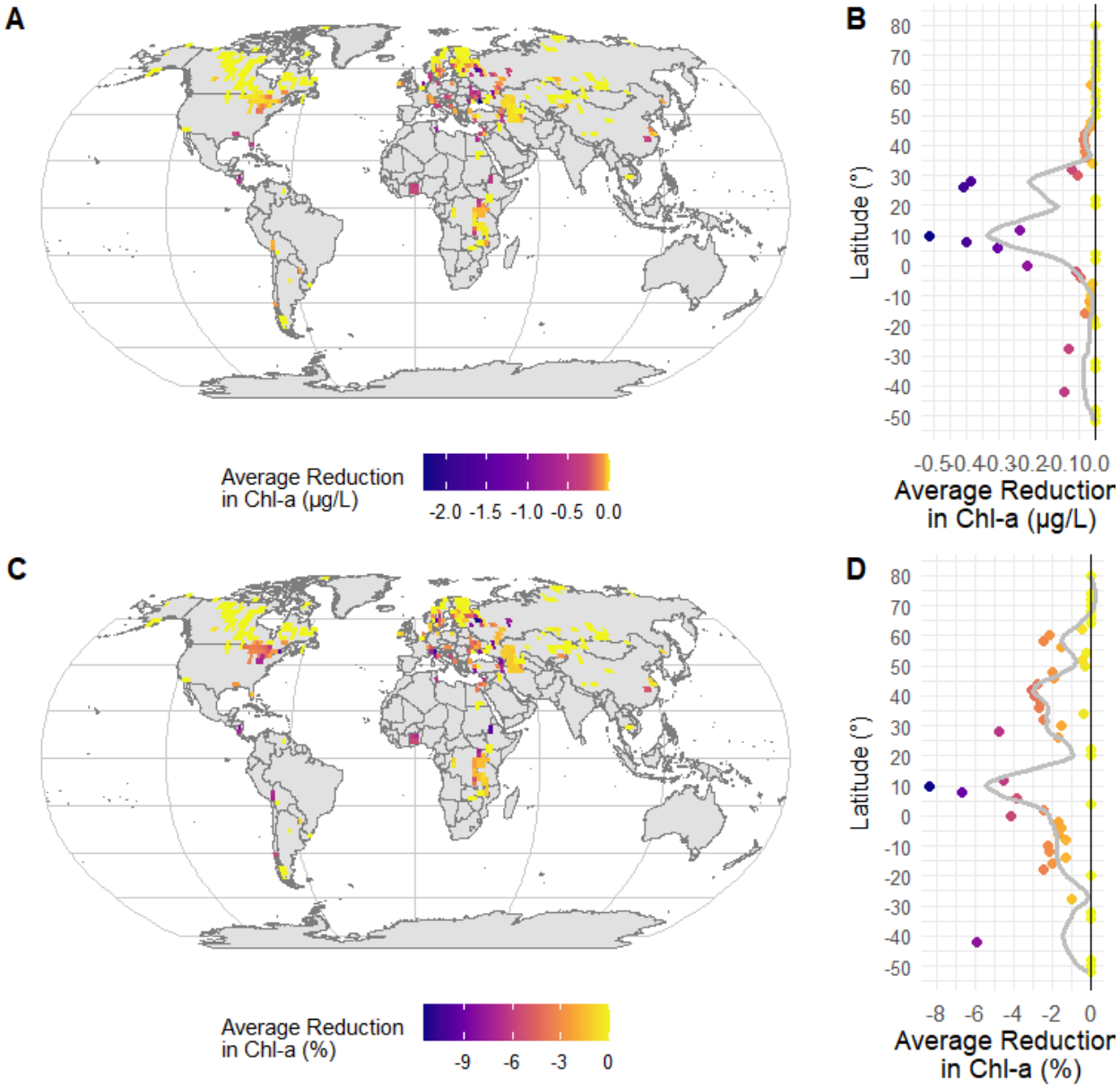

Figure S5 | Global latitudinal patterns of chlorophyll-a (chl-a) reduction associated with a 20% reduction in urban area extent. *(A) Global distribution of absolute chl-a reduction (µg/L) aggregated in 2° latitude-longitude bins, displayed in Robinson projection. (B) Latitudinal trends in absolute chl-a reduction, with a LOESS-smoothed line (span = 0.25) highlighting median changes. (C) Percent reduction in chl-a, similarly binned and projected. (D) Corresponding latitudinal trends for percent change. Data represent estimates based on aggregated global urban area extent records, with reductions calculated as the mean change per bin. Urban area*

extent correlates with greater chl-a reductions in highly urbanized mid-latitude regions (30°–50°), particularly in the Northern Hemisphere. Gray shading in maps represents landmasses; missing data indicate sparse sampling in polar and remote regions. Spatial aggregation and analysis performed in R using "sf"[44,45] and "ggplot2"[49] packages. Gray basemaps are from Natural Earth[71]. Watershed urban area data from LakeAtlas.[51] Bias-corrected lake chl-a data from Kraemer et al. (2022)[6].

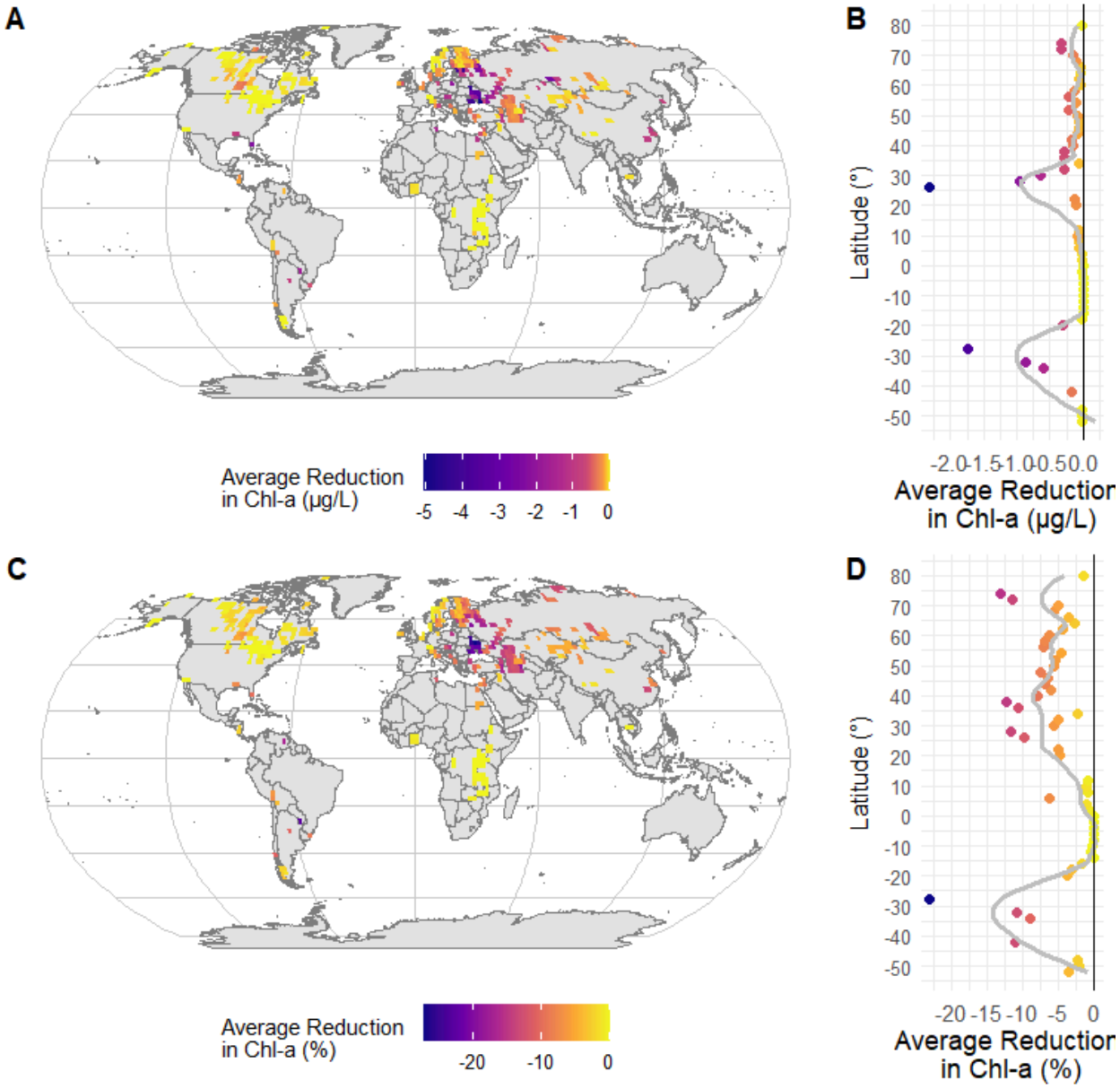

Figure S6 | Global latitudinal patterns of chlorophyll-a (chl-a) reduction associated with improvements in Human Development Index (HDI). *(A) Global distribution of absolute chl-a reduction (µg/L) aggregated in 2° latitude-longitude bins, displayed in Robinson projection. (B) Latitudinal trends in absolute chl-a reduction, with a LOESS-smoothed line (span = 0.25) highlighting median changes. (C) Percent reduction in chl-a, similarly binned and projected. (D) Corresponding latitudinal trends for percent change. Data represent estimates based on*

aggregated global HDI records, with reductions calculated as the mean change per bin. Improvements in HDI correlate with greater chl-a reductions in regions experiencing significant socioeconomic development, particularly at mid-latitudes (30°–50°) in the Northern Hemisphere. Gray shading in maps represents landmasses; missing data indicate sparse sampling in polar and remote regions. Spatial aggregation and analysis performed in R using "sf"[44,45] and "ggplot2"[49] packages. Gray basemaps are from Natural Earth[71]. Watershed HDI data from LakeAtlas.[51] Bias-corrected lake chl-a data from Kraemer et al. (2022)[6].

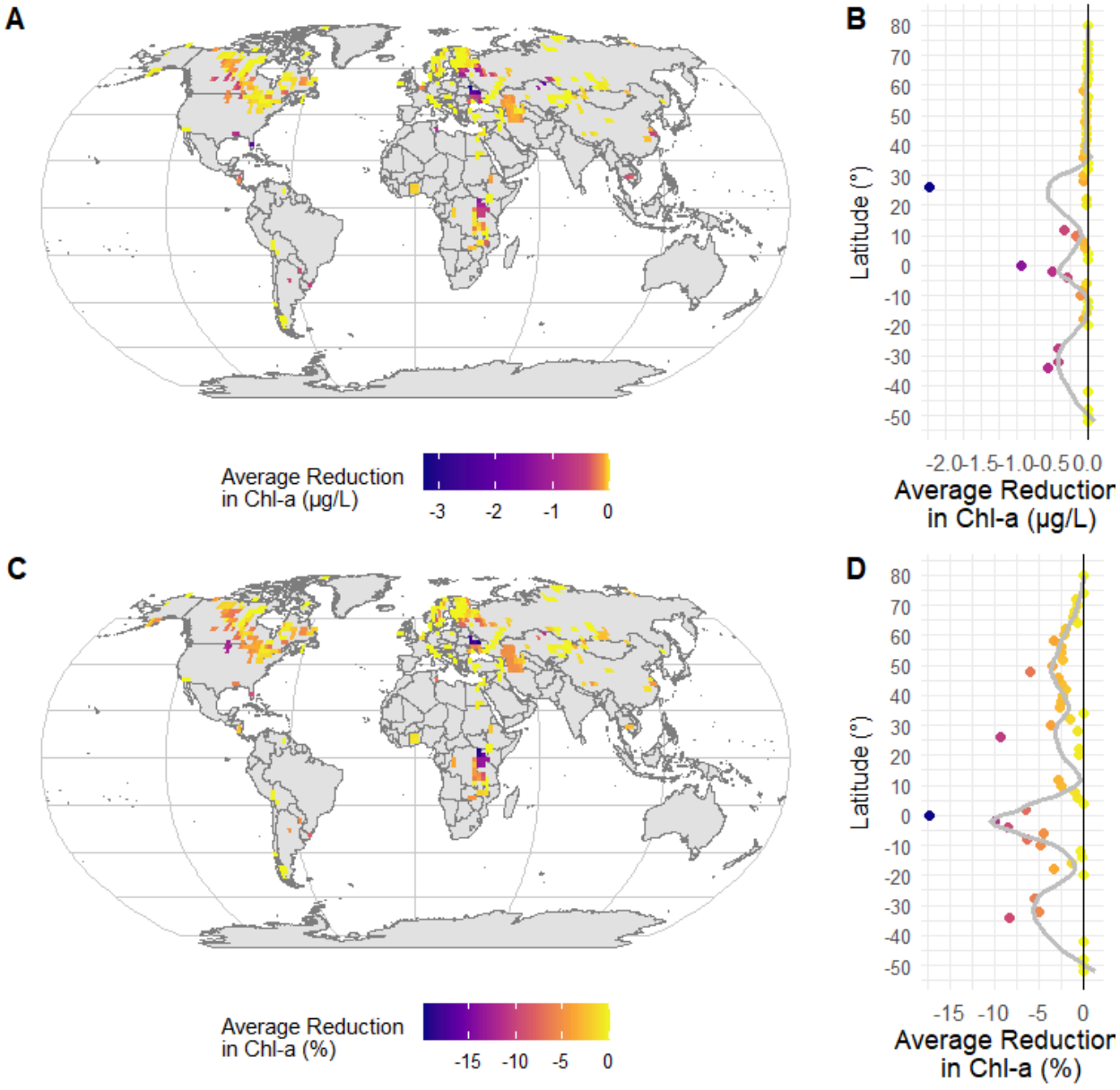

Figure S7 | Global latitudinal patterns of chlorophyll-a (chl-a) reduction associated with expanded wetland areas. (A) Global distribution of absolute chl-a reduction (µg/L) aggregated in 2° latitude-longitude bins, displayed in Robinson projection. (B) Latitudinal trends in absolute chl-a reduction, with a LOESS-smoothed line (span = 0.25) highlighting median changes. (C)

Percent reduction in chl-a, similarly binned and projected. (D) Corresponding latitudinal trends for percent change. Data represent estimates based on aggregated global wetland area records, with reductions calculated as the mean change per bin. Expanded wetland areas correlate with greater chl-a reductions, particularly in regions where wetlands effectively mitigate nutrient runoff, notably at mid-latitudes (30°–50°) in the Northern Hemisphere. Gray shading in maps represents landmasses; missing data indicate sparse sampling in polar and remote regions. *Spatial aggregation and analysis performed in R using "sf"*[44,45] *and "ggplot2"*[49] *packages. Gray basemaps are from Natural Earth*[71]*. Watershed wetland data from LakeAtlas.*[51] *Bias-corrected lake chl-a data from Kraemer et al. (2022)*[6]*.*

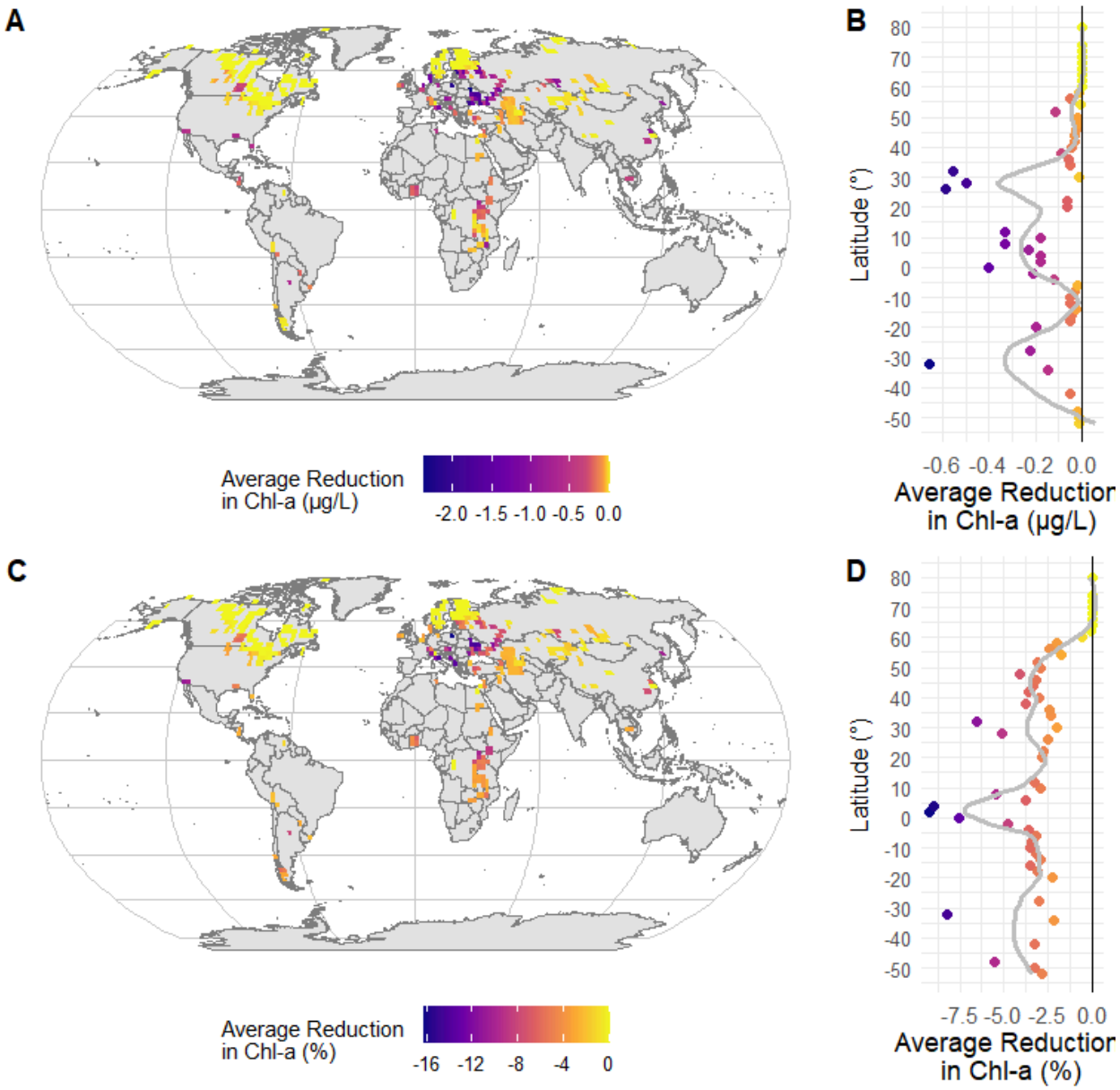

***Figure S8 | Global latitudinal patterns of chlorophyll-a (chl-a) reduction associated with a 20% reduction in pasture extent in each lake's watershed, relative to 2010 conditions.*.** *(A) Global distribution of absolute chl-a reduction (µg/L) aggregated in 2° latitude-longitude bins, displayed in Robinson projection. (B) Latitudinal trends in absolute chl-a reduction, with a LOESS-smoothed line (span = 0.25) highlighting median changes. (C) Percent reduction in chl-a, similarly binned and projected. (D) Corresponding latitudinal trends for percent change. Data are derived from aggregated coastal monitoring records, with reductions calculated as the mean change per bin. Pasture expansion correlates with greater chl-a declines at mid-latitudes (30°–50°), particularly in Northern Hemisphere coastal zones. Gray shading in maps represents landmasses; missing data reflect sparse sampling in polar and open-ocean regions. Spatial aggregation and analysis performed in R using "sf"[44,45] and "ggplot2"[49] packages. Gray basemaps are from Natural Earth[71]. Watershed pasture extent data from LakeAtlas.[51] Bias-corrected lake chl-a data from Kraemer et al. (2022)[6].*

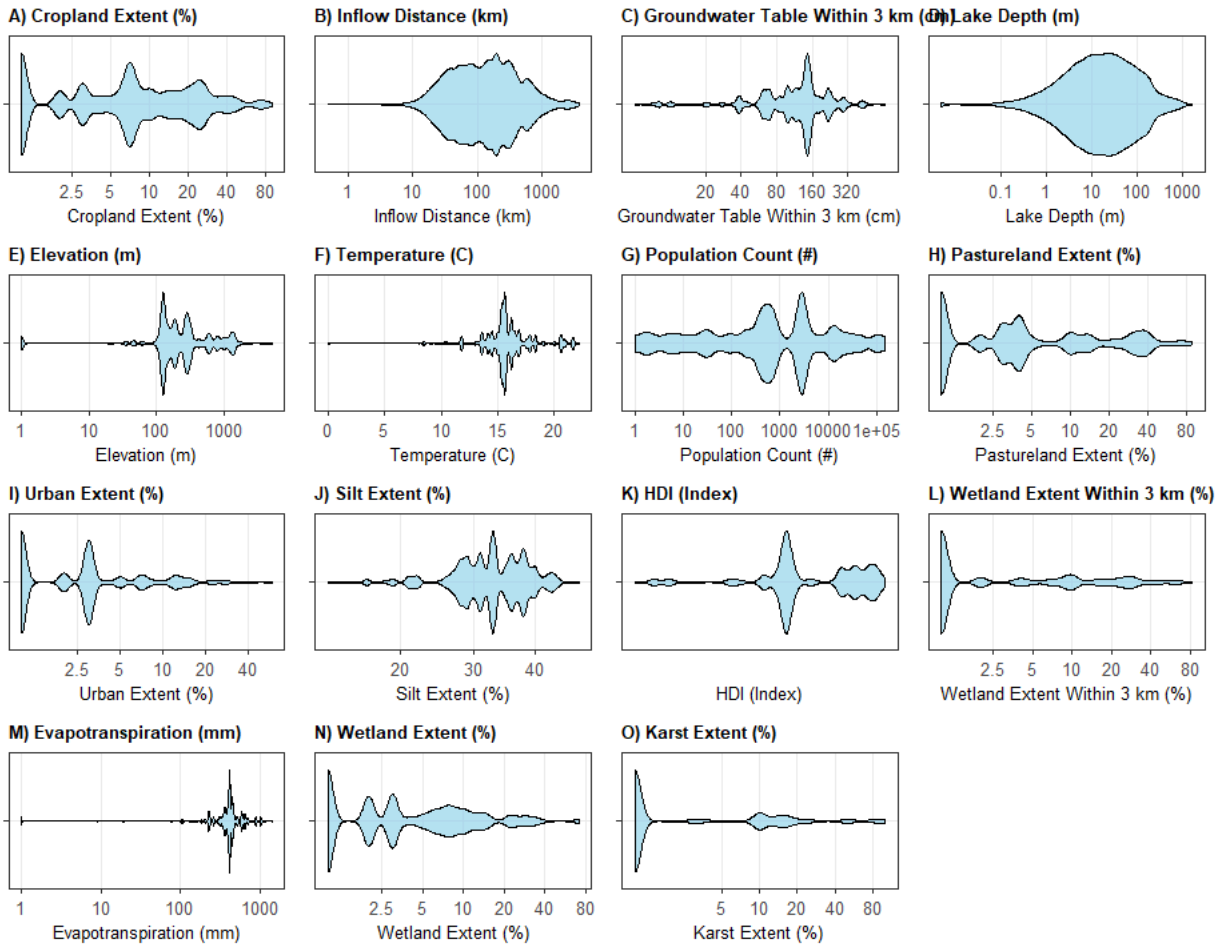

Figure S9 | Distributions of predictor variables used to model chlorophyll-a concentrations in lakes. *Each panel (A–O) shows the distribution of one of the 15 predictor variables included in the boosted regression tree (BRT) model for chlorophyll-a (µg/L).*

Predictors include cropland extent (%), groundwater table depth (cm), urban land cover (%), and lake depth (m), among others. Variables were transformed (logarithmic, square root, or squared) prior to modeling, but are displayed here using inverse-transformed axis labels to reflect values in their original units. Violin plots visualize the distribution of each predictor across hundreds of lakes globally. X-axes represent the untransformed variable values (e.g., % cover, meters, degrees Celsius), while spacing reflects the transformed scale used in the BRT model. Letters (A–O) in the panel titles correspond to variable order in supplementary tables. Data were derived from geospatial, hydrological, and socioeconomic datasets. Plots were generated in R using ggplot2, with consistent breaks and theming for cross-panel comparability.

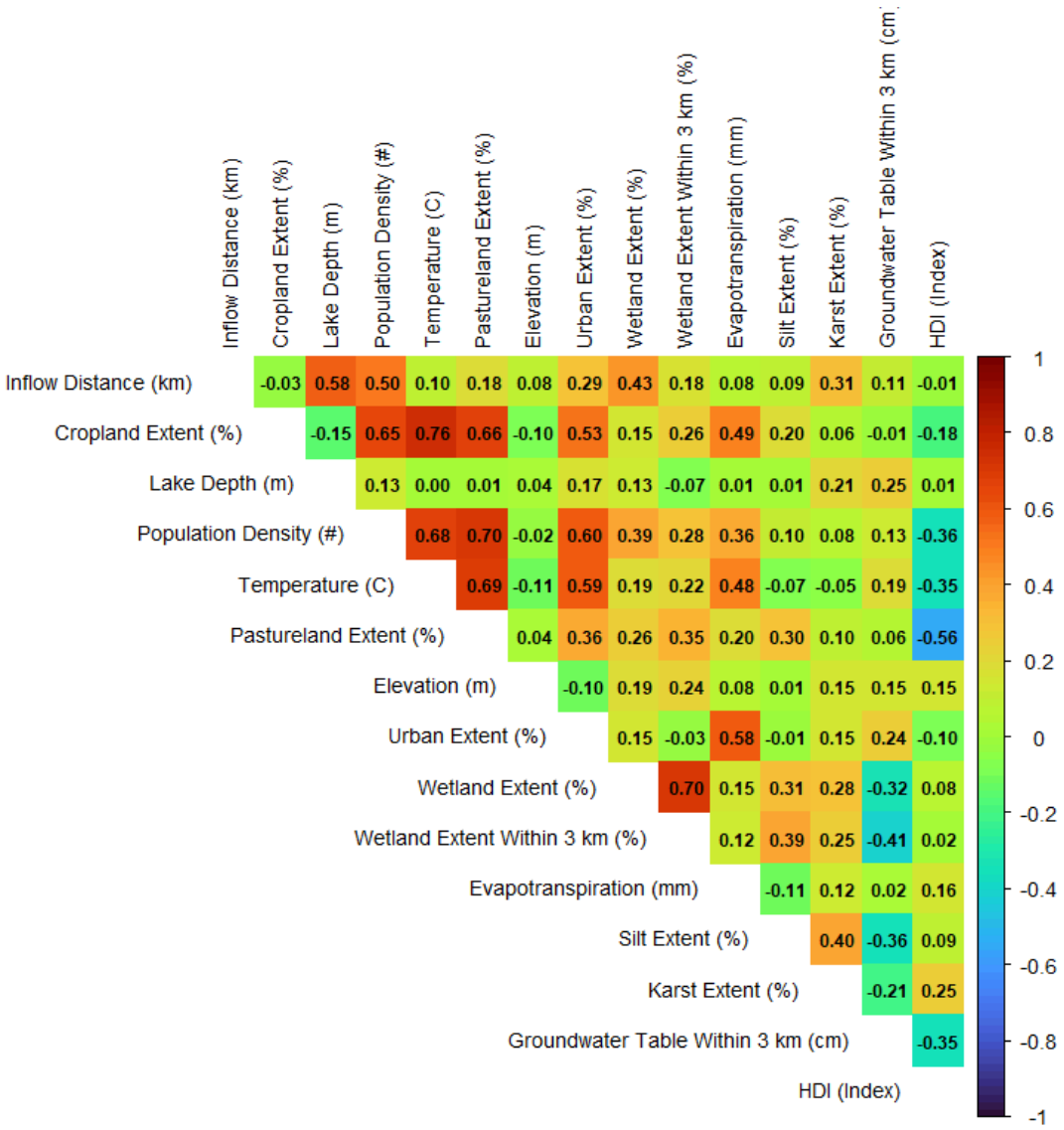

Figure S10 | Pairwise correlations among predictors in lake water quality analysis. *Kendall's tau correlation coefficients (ranging from -1 to 1) for 15 predictors of chlorophyll-a concentrations, including land use (cropland, urban, pasture), hydrological features (wetland extent, groundwater depth), and lake characteristics (depth, elevation). Coefficients are displayed in the upper triangle, colored using the turbo viridis scale (blue = negative, yellow = neutral, red = positive). Strongest positive correlations occurred between cropland and*

watershed air temperature (τ = 0.76). Predictors were log- or square root-transformed prior to analysis. Data were sourced from geospatial, hydrological, and socioeconomic datasets standardized across lakes. Correlations computed in R using "corrplot", with variable labels simplified for interpretability (e.g., "HDI (Index)" for Human Development Index).

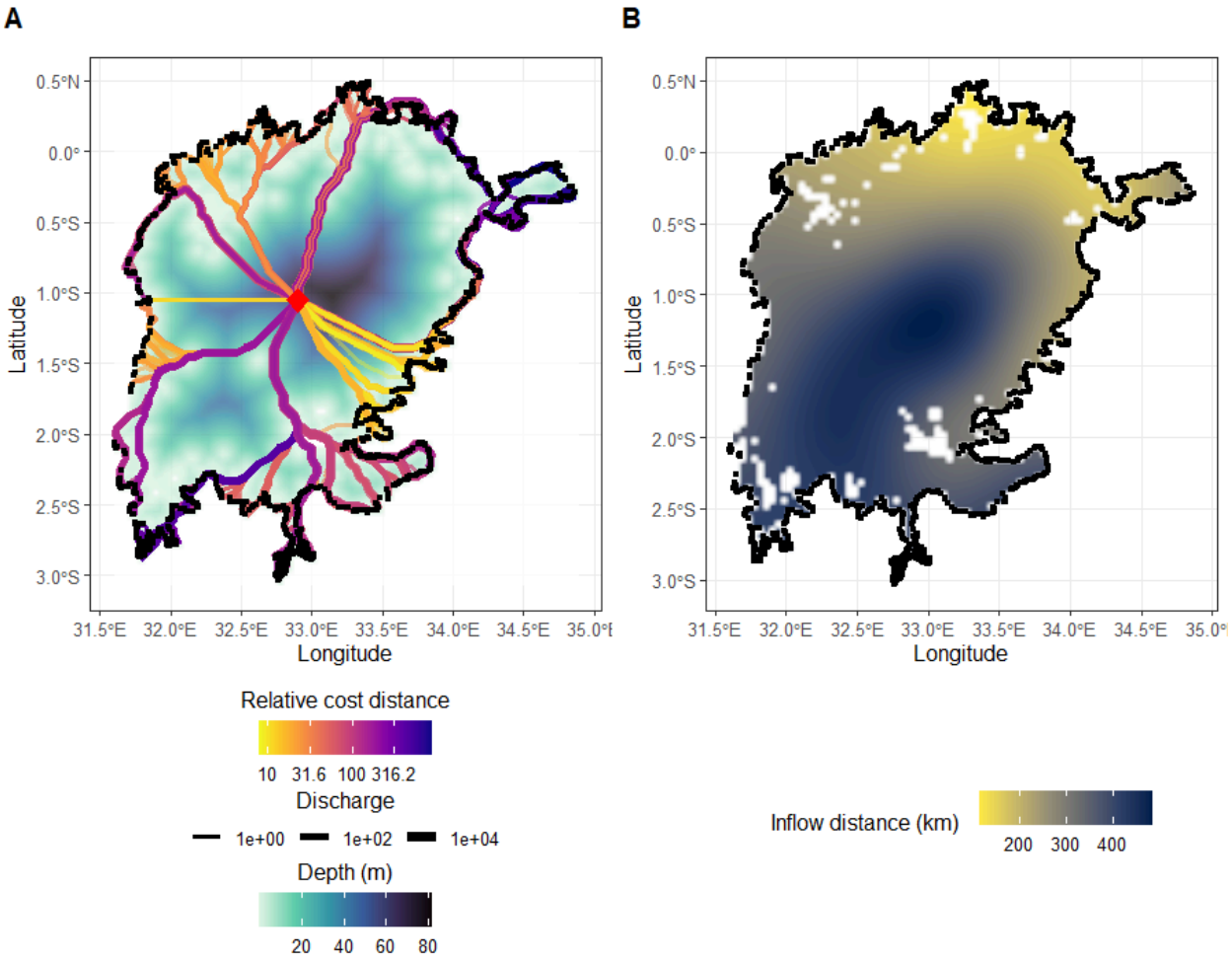

Figure S11 | Demonstration of the discharge-weighted inflow distance calculation for Lake Victoria, East Africa. *(A) Geoprocessing step illustrating the calculation of discharge-weighted inflow distance for a single, centrally located gridcell (red diamond). Depth values (m) were aggregated from a high-resolution raster [64]. Valid inlet points (black circles) connect to the central location via least-cost paths computed in R using a water depth-based transition function, which minimizes the volume of water traversed by each path. Path color indicates relative cost distance, and line width represents inlet discharge on a logarithmic scale. (B) Resulting spatial distribution of discharge-weighted inflow distances calculated for all locations within the lake. Raster colors represent inflow distances in kilometers, with darker shades indicating greater inflow distance. White spots on the map indicate no data associated with island locations within the lake. Legends for color scales and discharge values are positioned at the bottom for clarity.*